Charles University in Prague
Faculty of Mathematics and Physics

DIPLOMA THESIS

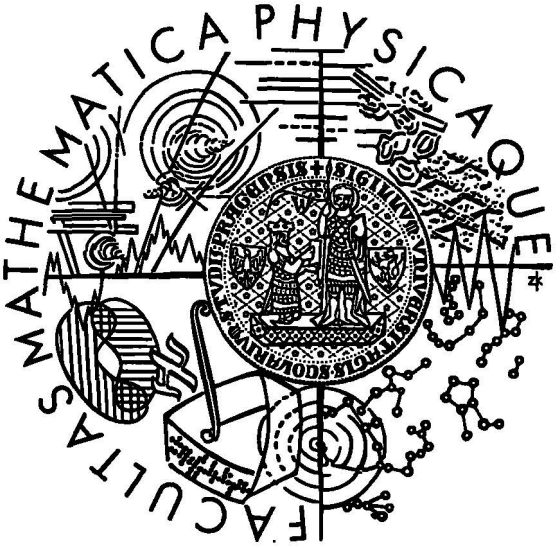

Jiří Minář

Study of spatial behaviour of photon pairs generated by parametric down-conversion

Department of Chemical Physics and Optics
Supervisor: Pavel Lipavský, CSc.
Advisor: doc. RNDr. Miloslav Dušek, Ph.D.
Study program: Physics
Study branch: Optics and optoelectronics

I would like to express my gratitude to the supervisors of my diploma thesis, Pavel Lipavský, CSc. and doc. RNDr. Miloslav Dušek, Ph.D. for their priceless support and help.

Prohlašuji, že jsem svou diplomovou práci napsal samostatně a výhradně s použitím citovaných pramenů. Souhlasím se zapůjčením práce.

V Praze dne Jiří Minář

Contents

Název práce: *Studium prostorových vlastností fotonových párů generovaných parametrickou sestupnou konverzí*
Autor: *Jiří Minář*
Katedra (ústav): *Katedra chemické fyziky a optiky*
Vedoucí diplomové práce: *Pavel Lipavský, CSc.*
E-mail vedoucího: *lipavsky@fzu.cz*

Abstrakt

Pokrok v optických experimentálních metodách umožnil zkoumat fenomén kvantové provázanosti v laboratorních podmínkách. Jedna z nových metod používá dvoufotonové stavy k měření závislostí mezi prostorovou a prostorově frekvenční oblastí, tj. veličin přímo spojených s Heisenbergovými relacemi neurčitosti. Účelem této diplomové práce je nalézt a poskytnout odpovídající popis skutečného experimentu.

Uvažovali jsme experiment s jedním fotonovým párem, kde se každý z fotonů šíří jiným zobrazovacím systémem. První z nich je tvořen spojnou čočkou, druhý pak dvouštěrbinou. Naším cílem bylo nalézt korelátor pro tento konkrétní experiment.

Ve skutečnosti již existuje zjednodušený model, který však nezahrnuje některé důležité realistické rysy experimentu. Vyvinuli jsme tedy model, který tyto rysy zahrnuje v aproximaci vedoucí na poloanalytický výsledek.

Podařilo se nám ukázat, že model poskytuje předpovědi, které jsou v dobré shodě s experimentálními daty. Zdá se tedy, že je použitelný pro předpovědi reálně prováděných experimentů tohoto typu.

Klíčová slova: *kvantová provázanost, parametrická sestupná konverze, Heisenbergův mikroskop*

Title: *Study of spatial behaviour of photon pairs generated by parametric down-conversion*
Author: *Jiří Minář*
Department: *Department of Chemical Physics and Optics*
Supervisor: *Dr. Pavel Lipavský*
Supervisor's e-mail address: *lipavsky@fzu.cz*

Abstract

The progress in optical experimental techniques made it possible to investigate quantum entanglement in laboratory conditions. One of the new methods uses two-photon states to measure the relationship between the wave vector domain and the space domain, i.e., quantities related by the Heisenberg relation of uncertainty. The presented diploma work is aimed to offer a convenient description of the real experiment.

We considered an experiment with one entangled photon pair, where each photon propagates in a separate imaging system. The first system contains the convergent lens, the other the double slit. Our aim was to evaluate the correlator of this particular experiment.

A simple theoretical model already exists, but it does not cover important realistic features of the experiment. We have developed a description, which involves these features in an approximation leading to semi-analytical theory.

As we have shown, our model provides us with predictions, which are in good agreement with experiment. Therefore it seems, that our model is suitable to predict the realistic results of this type of experiment.

Keywords: *quantum entanglement, parametric down-conversion, Heisenberg microscope*

Chapter 1

Motivation

We may begin with short explanation of the key word for the whole work, which is *quantum entanglement*. As stated in [1]: Quantum entanglement is a quantum mechanical phenomenon in which the quantum states of two or more objects have to be described with reference to each other, even though the individual objects may be spatially separated. This leads to correlations between observable physical properties of the systems. For example, it is possible to prepare two photons in a single quantum state such that when one is observed with the vertical polarization, the other one will always be observed with the horizontal polarization and vice versa. This holds despite the fact that it is impossible to predict, according to quantum mechanics, which set of measurements will be observed. As a result, measurements performed on one system seem to be instantaneously influencing other systems entangled with it.

There are several ways how to realize the phenomenon of quantum entanglement. One of the most common ones are optical experiments using an entangled photon pair. For historical reasons the two photons are called *idler* and *signal* photon. Both photons are normally specified by the well-known physical properties such as frequency, wave vector, wave length and polarization. We can ask ourselves how is the relationship among these variables in an entangled photon pair, having in mind that the entanglement is a new physical quality which introduces specific relationships between idler and signal photon.

Another important key word is *correlation* which is some specific relationship among two or more observable variables. A function describing the correlation is usually called a *correlator*. It is especially helpful to use the correlator for the experiments based on quantum entanglement. The importance of such a description could be seen from the examples discussed below. Basically, we can distinguish three different types of correlation between the two photons which are namely the correlation in

- polarizations
- frequencies
- space

The first one means, that, for example, if we measure the vertical polarization on the idler, we also measure the horizontal polarization on the signal and vice versa, exactly as it is described at the beginning of this chapter. But at this moment our interest isn't set on the experiments involving the polarization states of photons, so we neglect this type of correlation and we focus on the remaining two types.

The correlation in frequencies can be clearly understood from the next example. Consider a situation where the pump laser of frequency ω_0 impacts the crystal where the entangled photon pair is created (see *Figure 1.1*).

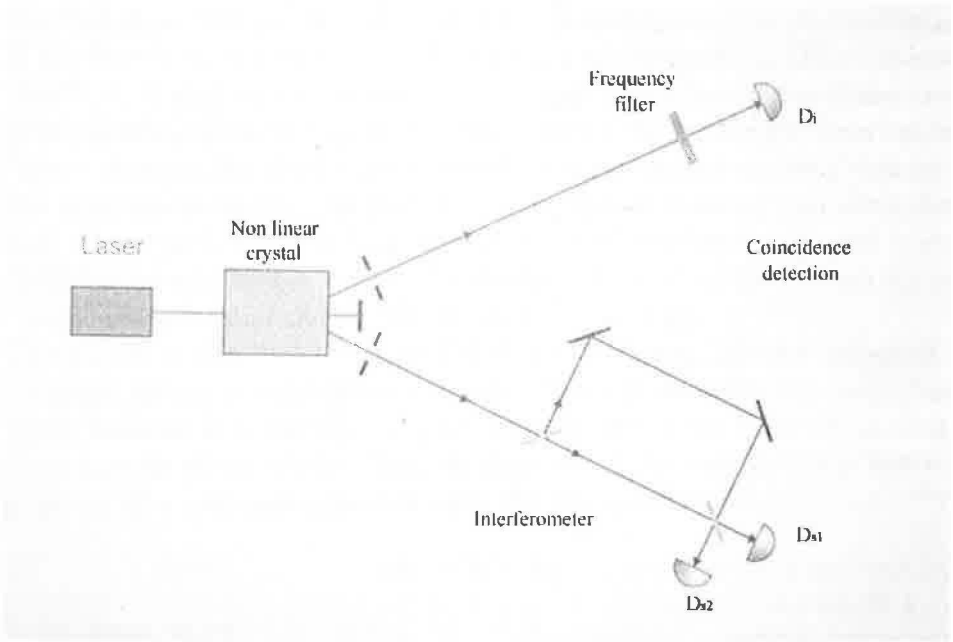

Figure 1.1: The scheme of experiment in the frequency domain. This picture is from Ref. [2].

Without any detailed explanation assume, that frequency of idler ω_i and frequency of signal ω_s respect following equation

$$\omega_0 = \omega_i + \omega_s$$

Next we assume that the state vector $|\psi)$ of signal and idler is described as

$$|\psi) = \int \mathrm{d}\omega_i \; \xi(\omega_i) \, |\omega_i\rangle \, |\omega_s\rangle$$

where $\xi(\omega_i)$ is a weight function. Let us denote the photon propagating in the upper branch as idler and the photon going through interferometer as signal. Normally, if the path difference between the two branches of Mach-Zehnder interferometer is bigger than the length of coherence, we cannot observe interference. However we can prolong the length of coherence (and hence renew the interference) by putting the frequency filter choosing a narrow set of frequencies in front of the interferometer. We should do this in the classical type of measurement, but in case of entangled photon pair (have again a brief look at the equations above) we accomplish this goal by putting the frequency filter to the path of idler in the upper branch! So finally the rate of coincidence between detectors D_i and D_{s1} or D_i and D_{s2} depends on the frequency transmissivity of the filter and on the path difference in the interferometer.

A number of such experiments has been already made in the frequency domain, see [3, 4, 5] and references in there, but one may ask whether there are some equivalent experiments in the space domain. Here we finally use the term *correlation in the space domain*, the third type of correlation mentioned above. Consider again a similar experiment as the one just described, but instead of frequency filter we introduce a lens performing a Fourier transform of incident beam and instead of Mach-Zehnder interferometer we insert a double slit creating the diffraction pattern in the image space behind the double slit (see *Figure 1.2*).

The aim is to measure the coincidence rate between the two detectors (*C.C.* in the scheme means a coincidence counter). We will describe this experiment in detail later, because it is exactly the goal of the entire thesis. Now let us focus only on general aspects of the whole affair. Analogously to the relationship between the frequencies of idler and signal we can write for the wave vectors

$$\mathbf{k}_0 = \mathbf{k}_i + \mathbf{k}_s$$

and for the state vector

$$|\psi) = \int \mathrm{d}\mathbf{k}_i \; F(\mathbf{k}_i) \, |\mathbf{k}_i\rangle \, |\mathbf{k}_s\rangle$$

where $F(\mathbf{k}_i)$ is a weight function. Note that the first equation involving three wave vectors is satisfied inside the crystal and has to be modified using the laws of refraction known from geometrical optics if one desires to describe this relationship outside the crystal.

When searching for analogies between the experiments in the frequency and space domain we can notice, that the function of frequency filter is performed by the position of detector in the upper branch. And so is the functionality of the detector behind the double slit - when changing its position we directly influence the rate

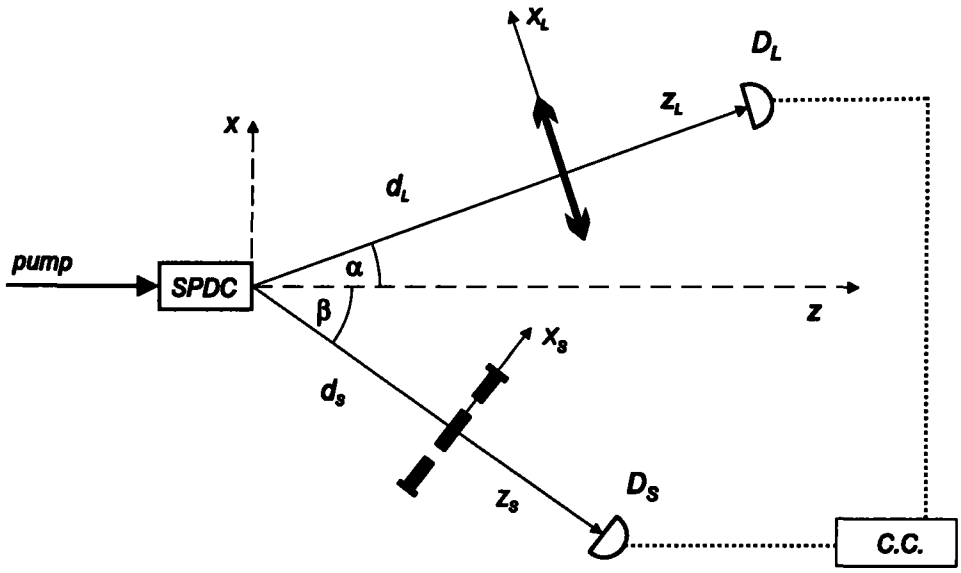

Figure 1.2: The scheme of experiment in the space domain.

of coincidence. Instead of the frequency transmissivity of the filter and the time delay between the two branches of Mach-Zehnder interferometer we have just the positions of detectors in the space. Thus we can see two interesting things at this moment - an analogy between the space and frequency domain experiments and the correlation between the space of wave vectors and the real space. By the latter property we mean that by setting up the position of the detector we directly choose one particular or a narrow set of wave vectors.

As one can see from the lines in this chapter, there are actually several important motivations for this work:

- We want to afflict analogies and differences between the experiments made in the temporal frequency domain and the experiments in the space frequency domain. The latter aren't so much experimentally explored.
- This work could serve as a theoretical support offering the exact description and prediction of measured quantities for this concrete experiment.
- Experiments on the entanglement test the quantum theory. We want to support this effort by a convenient theoretical analysis.
- Present development in the field of quantum information, which is very quick indeed, seems to match the very basic physical laws and principles and the very practical applications at the same time. Although this thesis is a basic

research work, it could potentially directly serve to some more practical and particular purpose.

Chapter 2

Theoretical model

Let suppose an experimental setup sketched in *Figure 1.2.* The incident laser beam impacts the non-linear medium which we take to be an anisotropic crystal with $\chi^{(2)}$ susceptibility. The parametric down-conversion occurs and we have two photons at the output from the crystal. We insert a convergent lens to the path of the first photon and we detect the resulting signal with a detector D_L. In the path of the second photon we put a double slit and detect the signal with a detector D_S. From now on, we will use the abbreviation L-branch for a branch including the lens and S-branch for a branch including the double slit. Our goal is to predict the correlation of signals from the two detectors.

2.1 Definitions

2.1.1 Light in the second quantization

To describe physical properties of light we will use an electric field $\mathbf{E}$. We will use the formalism of second quantization which is derived in most of textbooks on quantum mechanics such as [6, ch. 4] or [7, ch. X]. When manipulating Maxwell equations, we obtain

$$\mathbf{E}(\mathbf{r},t) = -\partial_t \mathbf{A}(\mathbf{r},t) - \nabla\phi(\mathbf{r},t) \tag{2.1}$$

where $\mathbf{A}$ is a vector potential and ϕ is an electric potential. Here we do not assume static electric fields, therefore we can use the gauge in which the scalar potential is zero,

$$\mathbf{E}(\mathbf{r},t) = -\partial_t \mathbf{A}(\mathbf{r},t)$$

In our model, the light propagating behind the crystal doesn't interact with matter any more (except of the detection itself).

After having quantized the electric field, we can separate it to its annihilation $(+)$ and creation $(-)$ parts

$$\mathbf{E}(\mathbf{r},t) = \mathbf{E}^{(+)}(\mathbf{r},t) + \mathbf{E}^{(-)}(\mathbf{r},t) \tag{2.2}$$

Using operators of second quantization, we can write for both components

$$\mathbf{E}^{(+)}(\mathbf{r},t) = \int \frac{\mathrm{d}\mathbf{k}}{(2\pi)^3}\, \mathbf{E}_\mathbf{k}(\mathbf{r})\; a_\mathbf{k}(t) \tag{2.3}$$

$$\mathbf{E}^{(-)}(\mathbf{r},t) = \int \frac{\mathrm{d}\mathbf{k}}{(2\pi)^3}\, \mathbf{E}^*_\mathbf{k}(\mathbf{r})\; a^\dagger_\mathbf{k}(t) \tag{2.4}$$

where

$$\mathbf{E}_\mathbf{k}(\mathbf{r}) = i\mathbf{e}\sqrt{\frac{\hbar\omega_k}{2\epsilon_0}}\, e^{i\mathbf{k}\mathbf{r}} \tag{2.5}$$

is a plane wave corresponding to the mode $\mathbf{k}$ and normalized to energy quantum $\hbar\omega_k$. $\mathbf{e}$ is unity polarization vector and ϵ_0 is permitivity of vacuum. The quantum field operators are normalized to Dirac δ-function

$$a_\mathbf{k} a^\dagger_\mathbf{q} - a^\dagger_\mathbf{q} a_\mathbf{k} = (2\pi)^3\, \delta(\mathbf{k}-\mathbf{q}) \tag{2.6}$$

More general description would include also the summation over different polarizations, but for simplicity we choose only one polarization. In order to further simplify the notation we also introduce a complex amplitude of electric field appropriate to mode $\mathbf{k}$

$$\mathbf{E}_{0\mathbf{k}} = i\mathbf{e}\sqrt{\frac{\hbar\omega_k}{2\epsilon_0}} \tag{2.7}$$

We little outrun our script now and will talk about an ideal representation of state vectors and operators. It is convenient to work in the Heisenberg representation. In the free space, Hamiltonian reads (2.8).

$$H = \int \frac{\mathrm{d}\mathbf{q}}{(2\pi)^3} \left(a_{\mathbf{q}}^{\dagger} a_{\mathbf{q}} + \frac{1}{2} \right) \hbar\omega_q \tag{2.8}$$

Time evolution of the annihilation operator is given by the Heisenberg equation. Then we can write

$$\frac{\mathrm{d}a_{\mathbf{k}}(t)}{\mathrm{d}t} = \frac{1}{i\hbar} [a_{\mathbf{k}}(t), H]$$

For Hamiltonian (2.8) we obtain

$$\begin{aligned} \frac{\mathrm{d}a_{\mathbf{k}}(t)}{\mathrm{d}t} &= \frac{1}{i\hbar} \int \frac{\mathrm{d}\mathbf{q}}{(2\pi)^3} \left(a_{\mathbf{k}} a_{\mathbf{q}}^{\dagger} a_{\mathbf{q}} - a_{\mathbf{q}}^{\dagger} a_{\mathbf{q}} a_{\mathbf{k}} \right) \hbar\omega_q \\ &= -i\omega_k a_{\mathbf{k}} \end{aligned}$$

This yields a result

$$a_{\mathbf{k}}(t) = a_{\mathbf{k}}(0) e^{-i\omega_k t} \tag{2.9}$$

Analogously for the creation operator we derive

$$a_{\mathbf{k}}^{\dagger}(t) = a_{\mathbf{k}}^{\dagger}(0) e^{i\omega_k t} \tag{2.10}$$

2.1.2 Correlator

When we want to involve a relationship between some physical variables, it is useful to introduce a variable called *correlator*. For further purposes we define a so-called *second-order correlator*.

Consider two electric fields $\mathbf{E}_L$ and $\mathbf{E}_S$ at coordinates $\mathbf{r}_L$ and $\mathbf{r}_S$. In our case, $\mathbf{r}_L$ is a position of an ideal point detector behind a lens, and $\mathbf{r}_S$ is a position of an ideal point detector behind a double slit.

We will measure the energy flow ($\sim E^2$) simultaneously at time t by both detectors. Expected coincidence is described by a second-order correlator, which is defined as

$$G_I(\mathbf{r}_L, t_L, \mathbf{r}_S, t_S) = \left\langle \mathbf{E}_L^{(-)}(\mathbf{r}_L, t_L) \mathbf{E}_S^{(-)}(\mathbf{r}_S, t_S) \mathbf{E}_S^{(+)}(\mathbf{r}_S, t_S) \mathbf{E}_L^{(+)}(\mathbf{r}_L, t_L) \right\rangle \tag{2.11}$$

where angular brackets denote averaging.

Generally, the averaging covers thermal and quantum noise. For simplicity, we assume only the quantum noise, therefore the mean value is taken in the spirit of quantum mechanics as the matrix element between state vectors.

For our purposes, it is advantageous to work in the Heisenberg representation. The time dependence of electrical fields is then fully covered by time dependence of field operators, while state vectors are stationary.

2.2 Spontaneous parametric down-conversion

Let us have a brief look at the process of Spontaneous Parametric Down Conversion (SPDC) and the properties of produced light. First, consider a sufficiently strong pump laser of frequency ω_0 and wave vector $\mathbf{k}_0$. The pump beam impacts on nonlinear medium, in which some of its photons convert to photon pairs. The two produced photons are usually called *signal* and *idler* photons. We will assume that signal goes to the double slit while idler goes to the lens.

We remind that we index all physical variables related to the lens with the letter L and variables related to the double slit with letter S. Accordingly, ω_L, ω_S, $\mathbf{k}_L$, $\mathbf{k}_S$ are the frequencies and wave vectors of photons in L-branch and S-branch .

It's not our goal to describe here the background of SPDC in detail but just pick-up some useful and interesting characteristics of this phenomenon. One can find more detailed information about SPDC eg. in [8, p. 1074].

In an ideal case we assume a steady state in which the energy conservation has the form

$$\omega_0 = \omega_L + \omega_S \tag{2.12}$$

Furthermore, considering an infinite nonlinear medium, the momentum conservation condition is satisfied

$$\mathbf{k}_0 = \mathbf{k}_L + \mathbf{k}_S \tag{2.13}$$

These two conservation laws link idler and signal photons.

Amplitudes of wave vectors depend on frequencies via dispersion relations

$$k_L = \frac{\omega_L}{c} n^{\omega_L} \qquad k_S = \frac{\omega_0 - \omega_L}{c} n^{\omega_S} \qquad k_0 = \frac{\omega_0}{c} n^{\omega_0} \tag{2.14}$$

where c is the speed of light in vacuum. The refractive index n depends on frequency specified in superscript. It is obvious that in order to satisfy the phase matching condition (2.13) all wave vectors must lay in the same plane. Then we can rewrite the phase matching condition in the following form (see *Figure 2.1*)

$$k_L \sin\alpha_L = k_S \sin\alpha_S \tag{2.15}$$

$$k_L \cos\alpha_L + k_S \cos\alpha_S = k_0 \tag{2.16}$$

Substituting the wave vectors from relations (2.14) we obtain a set of equations

$$\omega_L n^{\omega_L} \sin\alpha_L = (\omega_0 - \omega_L)\, n^{\omega_S} \sin\alpha_S \tag{2.17}$$

$$\omega_L n^{\omega_L} \cos\alpha_L + (\omega_0 - \omega_L)\, n^{\omega_S} \cos\alpha_S = \omega_0 n^{\omega_0} \tag{2.18}$$

With an ideal aperture we can choose a single angle α_L. The two photons are then uniquely determined. Indeed, the pump frequency ω_0 is known and so are the dependencies of refractive indices $n^{\omega_L} = n^{\omega_L}(\omega_L)$, $n^{\omega_S} = n^{\omega_S}(\omega_0 - \omega_L)$, respectively. We

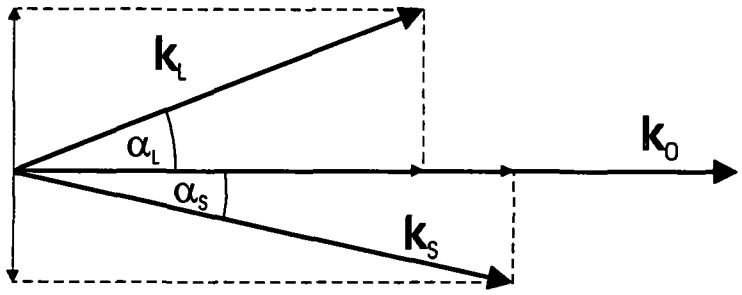

Figure 2.1: Phase matching condition in the crystal.

have a set of two equations for two unknown variables ω_S and α_S which yields the unique assignment between the chosen angle α_L and the other variables (frequencies, wave vectors, angle α_S) of the generated photons. In this case we talk about $\delta-$*correlations* in wave vectors which is the consequence of an assumption of quasi-infinite crystal. A realistic case of finite crystal and chopped laser beam is discussed below in this section.

2.2.1 Hamiltonian

There are several approaches to the SPDC. Probably the simplest one is a three mode description (which means the pump, idler and signal photon, each represented by a monochromatic plane wave). This approach provides us with some useful results, but still remains an idealization unable to involve some more real experiments.

In this thesis we want to study how robust is the correlation between idler and signal photons with respect to non ideal devices. We thus need the multi mode perturbative treatment which allows us to include following realistic features of our experiment - the chopped pump beam, a finite beam width, and a finite width of slab of the nonlinear medium. Each photon from the entangled pair is then represented by a wave packet including a range of possible wave vectors.

For our purposes we take the interaction Hamiltonian H_I from [8, p. 1080]

$$H_I = \int \frac{\mathrm{d}\mathbf{k}_L}{(2\pi)^3}\frac{\mathrm{d}\mathbf{k}_S}{(2\pi)^3}\chi^{(2)}_{\mathbf{k}_0,\mathbf{k}_L,\mathbf{k}_S}\int_V \mathrm{d}V\left[\mathbf{V}(\mathbf{r},t)e^{-i(\mathbf{k}_L+\mathbf{k}_S)\mathbf{r}}\right] e^{i(\omega_L+\omega_S-\omega_0)t}a^\dagger_{\mathbf{k}_L}a^\dagger_{\mathbf{k}_S} + h.c. \tag{2.19}$$

where V is a volume of the active region of the non-linear medium, $\mathbf{V}(\mathbf{r},t)$ is an amplitude of a pump laser. For simplicity, we omitted the summation over different polarizations. The integration is taken over all possible values of wave vectors $\mathbf{k}_L$ and $\mathbf{k}_S$.

As one can see, the expression (2.19) is rather complicated. First a), we demonstrate the treatment on the simplest model, where we take the pump beam to be a monochromatic plane wave and the slab is infinite. Second b), we discuss a general case with some convenient approximations.

a) monochromatic plane wave

We denote the volume integral as I. In the simplest case we suppose the incident pump laser beam to be a monochromatic plane wave, i.e., there is no chopping

$$\mathbf{V}(\mathbf{r},t) = \mathbf{V}_0 e^{i\mathbf{k}_0\mathbf{r}} \tag{2.20}$$

Moreover we assume, that the active region of non-linear medium is large enough so that the integration can be made over the whole space

$$\begin{aligned} I &= \int_{-\infty}^{\infty}\int_{-\infty}^{\infty}\int_{-\infty}^{\infty} \mathrm{d}x\mathrm{d}y\mathrm{d}z \mathbf{V}_0 e^{i(\mathbf{k}_0-\mathbf{k}_L-\mathbf{k}_S)\mathbf{r}} \\ &= \mathbf{V}_0\, 2\pi\,\delta\left(k_{0x}-k_{Lx}-k_{Sx}\right) 2\pi\,\delta\left(k_{0y}-k_{Ly}-k_{Sy}\right) 2\pi\,\delta\left(k_{0z}-k_{Lz}-k_{Sz}\right) \\ &= \mathbf{V}_0\,(2\pi)^3\delta\left(\mathbf{k}_0-\mathbf{k}_L-\mathbf{k}_S\right) \end{aligned} \tag{2.21}$$

The infinite volume integral leads to δ-functions, which exactly corresponds to the phase matching condition (2.13).

In this case of quasi-infinite crystal we also talk about so-called $\delta-$*correlations* between wave vectors. The origin of this name is clear. Here we should notice that the phase matching condition is fully accomplished, therefore there is no smearing in wave vectors. But how the situation changes if we consider a finite crystal, or at least the crystal finite in some dimension? Let us see next part of this section.

b) chopped gaussian beam in a finite slab

Consider a gaussian beam propagating along the z-axis, which is characterized by the equation [9]

$$\begin{aligned} \mathbf{V}(\mathbf{r},t) = \ & \frac{\mathbf{V}_0}{z+iz_0} e^{-ik_0\frac{x^2+y^2}{2(z+iz_0)}} e^{ik_0 z} && \text{for} \quad -\tau/2 < t < \tau/2 \\ & 0 && \text{elsewhere} \end{aligned} \tag{2.22}$$

where z_0 is the Rayleigh length of a gaussian beam. We assume that individual pulses of chopped light are sufficiently separated so that it is plausible to work with a single pulse of duration τ.

The gaussian profile of the pump beam and space limitation of the crystal bring some new aspects to the problem. A meaningful physical approximation can be achieved considering the following. The gaussian beam propagates along the z-axis in the crystal of length L. The width (or half-width) of the beam is very small

compared to the transversal extent of the crystal, so the integration could be taken over the whole cross plane. This yields to the volume integral

$$I = \int_{-\infty}^{\infty}\int_{-\infty}^{\infty}\int_{-L/2}^{L/2} \mathrm{d}x\mathrm{d}y\mathrm{d}z \frac{\mathbf{V}_0}{z+iz_0} e^{-ik_0\frac{x^2+y^2}{2(z+iz_0)}} e^{i(\mathbf{k}_0-\mathbf{k}_L-\mathbf{k}_S)\mathbf{r}} \tag{2.23}$$

After a long but straightforward calculation we receive for the spatial component of Hamiltonian

$$I = -2\pi i \frac{\mathbf{V}_0}{k_0} e^{Kz_0} \frac{\sin\left[\frac{1}{2}\left(k_0 - k_{Lz} - k_{Sz} - K\right)L\right]}{\frac{1}{2}\left(k_0 - k_{Lz} - k_{Sz} - K\right)} \tag{2.24}$$

where

$$K = -\frac{\left(k_{Lx}+k_{Sx}\right)^2 + \left(k_{Ly}+k_{Sy}\right)^2}{2k_0}$$

Out of interval $-\tau/2 < t < \tau/2$, I is zero. In x and y directions, we have found gaussian functions, which can be viewed as smeared δ-functions. In the z direction the smearing by *sinc*-function results.

2.2.2 State vector

Now we are ready to evaluate the state vector. We suppose the initial state of the system to be a vacuum state $|\psi(0)\rangle = |vac\rangle$. For $\tau c \gg L$ we can neglect propagation of the pulse through the non-linear medium and simply assume, that the pump pulse acts on the crystal in time interval $-\tau/2 < t < \tau/2$. After the action of the pump pulse, the state vector in the Dirac interaction representation is time independent and reads

$$|\psi\rangle = \exp\left[\frac{1}{i\hbar}\int_{-\tau/2}^{\tau/2} \mathrm{d}t' H_I(t')\right]|vac\rangle \tag{2.25}$$

For $t > \tau/2$ the Heisenberg and Dirac representations become identical. The pulse duration τ is long enough that our detection happens during the action of the pump pulse. Since we neglect possible reflections of the light from double slit or lens, we can describe the experiment in two steps. After expanding the exponential in (2.25) we neglect higher order terms, i.e., we assume, that the pump light generates a single photon pair, which leaves the crystal. Second, the photon pair is used as an initial condition for the calculation of the correlated detection on the lens and the double slit.

For the *non normalized* state vector we have

$$|\psi\rangle = |vac\rangle + \\ + \frac{1}{i\hbar}\int \frac{\mathrm{d}\mathbf{k}_L}{(2\pi)^3}\frac{\mathrm{d}\mathbf{k}_S}{(2\pi)^3}\chi^{(2)}_{\mathbf{k}_0,\mathbf{k}_L,\mathbf{k}_S} I \frac{\sin\left[\frac{1}{2}(\omega_0-\omega_L-\omega_S)\tau\right]}{\frac{1}{2}(\omega_0-\omega_L-\omega_S)} a^\dagger_{\mathbf{k}_L} a^\dagger_{\mathbf{k}_S}|vac\rangle + \ldots \tag{2.26}$$

where I is the volume integral in the Hamiltonian (2.19) labored in the previous section. The main contribution to the state vector comes from the pure vacuum state, which occurs with the highest probability in the real experiment, but does not contribute to the correlator. For simplicity of notation we will ignore the vacuum component (which does not contribute to the coincidence detection) writing the state vector as

$$|\psi\rangle = \int \frac{\mathrm{d}\mathbf{k}_L}{(2\pi)^3}\frac{\mathrm{d}\mathbf{k}_S}{(2\pi)^3} F(\mathbf{k}_L,\mathbf{k}_S) a^\dagger_{\mathbf{k}_L} a^\dagger_{\mathbf{k}_S}|vac\rangle \tag{2.27}$$

We have also neglected contributions of the higher order terms in the expansion of exponential, i.e. we neglected the creation of four and more entangled photons at the same time. The contribution of each mode to the whole state vector is described by a weight function

$$F = \frac{1}{i\hbar}\chi^{(2)}_{\mathbf{k}_0,\mathbf{k}_L,\mathbf{k}_S} I \frac{\sin\left[\frac{1}{2}(\omega_0-\omega_L-\omega_S)\tau\right]}{\frac{1}{2}(\omega_0-\omega_L-\omega_S)} \tag{2.28}$$

Deriving the above relations we tacitly supposed that the same refraction index holds in the whole space. In reality, this is not true. In the nonlinear medium the refraction index depends on frequency with values about $n = 1.5$, while in the air $n = 1$. The discontinuity in refraction index leads to two effects. First, the reflection on the slab surfaces modifies the amplitude of the pump beam. Moreover a backward component $e^{-i\mathbf{kr}}$ appears. Second, the refraction on the interface between crystal and air changes the direction of generated photons. Both these effects are neglected.

We suppose that the process of SPDC is satisfied if we use the phase matching of the first kind, E-OO, which means that the pump beam respect the extraordinary refraction index n_e, while both vectors $\mathbf{k}_L$, $\mathbf{k}_S$ respect the *ordinary* refractive index n_o. In principle the change of wave vectors of generated photons can be accounted for with the help of Snell's law. For simplicity we do not introduce this correction and assume the refractive index n_o applies to the whole space.

2.3 Fresnel diffraction

The major phenomenon we meet when describing our experiment is *diffraction*. The complete description of diffraction is not however so easy, but we can proceed with our work if we choose some appropriate approximation. For the assumed setup, we can use the so-called *Fresnel diffraction*.

Assume a space separated into two parts by a screen. This screen is nontransparent except the aperture. We know an electric field incident on the screen. We want to express the value of electric field in any point behind the aperture, i.e., in the place where we put our detector.

According to the Huygens principle, for an incident plane wave of wave vector $\mathbf{k}$, the field is given by the integral over the area Σ of aperture [10, p. 58]

$$\mathbf{E}(x_0, y_0) = \frac{1}{i\lambda} \iint_{\Sigma} \mathrm{d}x\mathrm{d}y\, \mathbf{E}(x, y) \frac{e^{ikr}}{r} \cos(\theta) \tag{2.29}$$

where $2\pi/\lambda = k = |\mathbf{k}|$ and $\mathbf{E}(x, y)$ is the value of incident field in the aperture. θ is the angle between vector $\mathbf{n}$ normal to the aperture and vector $\mathbf{r}$ connecting the point of radiation $[x, y, 0]$ and the point of detection $[x_0, y_0, z]$, and $r = |\mathbf{r}|$.

Further simplification can be accomplished by expanding the distance r as

$$\begin{aligned} r &= \sqrt{z^2 + (x_0 - x)^2 + (y_0 - y)^2} \\ &= z\sqrt{1 + \left(\frac{x_0 - x}{z}\right)^2 + \left(\frac{y_0 - y}{z}\right)^2} \\ &\approx z\left(1 + \frac{1}{2}\left(\frac{x_0 - x}{z}\right)^2 + \frac{1}{2}\left(\frac{y_0 - y}{z}\right)^2\right) \end{aligned} \tag{2.30}$$

which holds if z is much larger than a characteristic size of the aperture, $z^2 \gg x^2 + y^2$, and the detector position is close to the z-axis, $z^2 \gg x_0^2 + y_0^2$. Under these conditions

$$\frac{e^{ikr}}{z} \approx \frac{e^{ikz} e^{\frac{ik}{2z}\left[(x_0 - x)^2 + (y_0 - y)^2\right]}}{z} \tag{2.31}$$

where we approximated the distance r in the denominator by the distance z. In the phase factor we have to keep the lowest order correction, because of the large value of k, which causes the change of phase by large multiples of π.

In the spirit of the Fresnel approximation, we can ignore the cosine in the integral

$$\cos(\theta) = \frac{\mathbf{n} \cdot \mathbf{r}}{r} \approx \frac{z}{z} = 1 \tag{2.32}$$

Finally we have

$$\mathbf{E}(x_0, y_0) = \frac{e^{ikz}}{i\lambda z} e^{\frac{ik}{2z}(x_0^2+y_0^2)} \iint_{\Sigma} \mathrm{d}x\mathrm{d}y\, \mathbf{E}(x, y) e^{\frac{ik}{2z}(x^2+y^2)} e^{-\frac{ik}{z}(x_0 x + y_0 y)} \tag{2.33}$$

This can be rewritten in the equivalent form

$$\mathbf{E}(x_0, y_0) = \frac{e^{ikz}}{i\lambda z} e^{\frac{ik}{2z}(x_0^2+y_0^2)} \iint_{-\infty}^{\infty} \mathrm{d}x\mathrm{d}y\, t(x, y)\mathbf{E}(x, y) e^{\frac{ik}{2z}(x^2+y^2)} e^{-\frac{ik}{z}(x_0 x + y_0 y)} \tag{2.34}$$

where $t(x, y)$ is the function of transmission of the aperture. This form is more suitable for the approximations we introduce below.

2.4 Transforming properties of lens

In this part we will describe the Fourier transforming properties of a convergent lens. In fact we will consider a system consisting of an aperture just in the back plane of a lens and an ideal convergent lens. As one can guess, we have to describe two major phenomena. These are the Fourier transform performed by a lens and the Fresnel diffraction on the aperture.

2.4.1 Fourier transforming properties of lens

We assume a lens which has a refractive index n. The total phase shift of the light beam entering the lens at coordinates $[x, y]$ reads

$$\phi(x,y) = kn\Delta(x,y) + k\left[\Delta_0 - \Delta(x,y)\right] \tag{2.35}$$

where $\Delta(x,y)$ is the thickness of the lens at coordinates $[x,y]$ and Δ_0 is the maximum thickness of the lens. $kn\Delta(x,y)$ is the phase delay introduced by the lens and $k\left[\Delta_0 - \Delta(x,y)\right]$ is the phase delay introduced by the remaining free space. In order to find Δ as the function of coordinates, we consider a convergent lens consisting of two spherical surfaces of radius R_1, R_2 respectively. The thickness function is

$$\Delta(x,y) = \Delta_1(x,y) + \Delta_2(x,y) \tag{2.36}$$

where

$$\Delta_1 = \Delta_{01} - \left(R_1 - \sqrt{R_1^2 - (x^2+y^2)}\right) = \Delta_{01} - R_1\left(1 - \sqrt{1 - \frac{x^2+y^2}{R_1^2}}\right) \tag{2.37}$$

$$\Delta_2 = \Delta_{02} - \left(R_2 - \sqrt{R_2^2 - (x^2+y^2)}\right) = \Delta_{02} - R_2\left(1 - \sqrt{1 - \frac{x^2+y^2}{R_2^2}}\right) \tag{2.38}$$

Furthermore we assume that $R_j \gg x, y; j = 1,2$ so we can approximate the square roots in (2.37), (2.38) by the first two members of their binomial expansion

$$\sqrt{1 - \frac{x^2+y^2}{R_j^2}} \cong 1 - \frac{x^2+y^2}{2R_j^2} \qquad j = 1,2$$

Using this so-called *paraxial approximation* we obtain for the thickness function

$$\Delta(x,y) = \Delta_0 - \frac{x^2+y^2}{2}\left(\frac{1}{R_1} + \frac{1}{R_2}\right) \tag{2.39}$$

The phase factor (2.35) thus becomes

$$\phi(x,y) = k\Delta_0 + k(n-1)\Delta(x,y) = kn\Delta_0 - \frac{k}{2f}\left(x^2+y^2\right) \tag{2.40}$$

where f defined by

$$\frac{1}{f} \equiv (n-1)\left(\frac{1}{R_1}+\frac{1}{R_2}\right)$$

is the focal length of a lens.

Briefly, the lens introduces a phase shift $\phi(x,y)$ to the light propagating through the lens. If the electric field in the front plane of a lens is $\mathbf{E}$, we can write for the resulting electric field $\mathbf{E}'$ in the back plane of the lens

$$\mathbf{E}'(x,y) = \mathbf{E}(x,y)e^{\pm i\phi(x,y)} \tag{2.41}$$

where the sign in the exponent depends on the definition of $\mathbf{E}$. For example, if we take the electric field $\mathbf{E}$ to be a monochromatic plane wave with a negative phase factor $e^{-i(\omega t-\mathbf{kr})}$ we should use a positive sign in (2.41) and vice-versa. If we consider just mentioned sign convention, we can rewrite (2.41)

$$\mathbf{E}'(x,y) = \mathbf{E}(x,y)e^{ikn\Delta_0}e^{-\frac{ik}{2f}\left(x^2+y^2\right)} \tag{2.42}$$

The constant phase factor $e^{ikn\Delta_0}$ has no impact on the observed quantities and will be neglected hereafter.

2.4.2 Field distribution at detection plane

Now we turn to a situation when a monochromatic plane wave is incident on the lens of aperture. The question is how the distribution of electric field looks in a plane at distance z behind the lens. In order to prepare notation which distinguishes the lens and the double slit, we will index the variables attached to the lens by letter L, thus a distance of a detection plane from a lens $z \rightarrow z_L$, position of detector $[x_0,y_0] \rightarrow [x_L,y_L]$ and electric field $\mathbf{E}(x_0,y_0) \rightarrow \mathbf{E}_L(x_L,y_L)$. The electric field behind the lens is the incident field of the aperture, therefore

$$\mathbf{E}_L(x_L,y_L) = \frac{e^{ik_Lz_L}}{i\lambda_Lz_L}e^{\frac{ik_L}{2z_L}\left(x_L^2+y_L^2\right)}\iint_\Sigma \mathrm{d}x\mathrm{d}y\,\mathbf{E}'(x,y)e^{\frac{ik_L}{2z_L}\left(x^2+y^2\right)}e^{-\frac{ik_L}{z_L}(x_Lx+y_Ly)}$$

Writing the aperture in terms of the transmission $t(x,y)$ and using (2.42), we find

$$\begin{aligned}\mathbf{E}_L(x_L, y_L) &= \frac{\mathrm{e}^{ik_L z_L}}{i\lambda_L z_L} e^{\frac{ik_L}{2z_L}(x_L^2+y_L^2)} \\ &\times \iint_{-\infty}^{\infty} \mathrm{d}x\mathrm{d}y\, t(x,y)\mathbf{E}(x,y) e^{\frac{ik_L}{2}(x^2+y^2)\left(\frac{1}{z_L}-\frac{1}{f}\right)} e^{-\frac{ik_L}{z_L}(x_L x+y_L y)}\end{aligned} \tag{2.43}$$

This result is valid for a general distance z_L, provided that the Fresnel approximation holds true. However, it is advantageous to make detection in the focal plane. Why just the focal plane instead of a plane in general distance z_L ? There are two main reasons. First, the lens acts actually as an optical processor transforming the incident field to its Fourier image right in the lens' focal plane. The second reason is more or less technical. Obviously, if $z_L = f$, we get rid of the quadratic factor in integral and thus significantly simplify the calculation of electric field.

2.4.3 Infinite lens

In this section we will consider an idealistic lens with an infinite aperture, i.e., $t = 1$. We will find out how the lens affects an incident monochromatic plane wave of wave vector $\mathbf{k}_L$

$$\mathbf{E}(x,y) = \mathbf{E}_0^L\, \mathrm{e}^{ik_{Lz}d_L}\, \mathrm{e}^{i(k_{Lx}x+k_{Ly}y)} = \mathbf{E}_0^L\, \mathrm{e}^{ik_{Lz}d_L}\, \mathrm{e}^{i\mathbf{k}_L\mathbf{r}} \tag{2.44}$$

The phase factor $\mathrm{e}^{ik_{Lz}d_L}$ represents the phase shift between the source of radiation and the lens separated by the distance d_L. Within this section, this is an unimportant factor.

We express the wave vector in the spherical coordinates

$$k_{Lx} = k_L \sin\theta\cos\xi \tag{2.45}$$
$$k_{Ly} = k_L \sin\theta\sin\xi \tag{2.46}$$
$$k_{Lz} = k_L \cos\theta \tag{2.47}$$

Our goal is to find the electric field in *focal plane* of a lens. Substituting to the integral (2.43) we obtain

$$\mathbf{E}_L(x_L, y_L) = \mathbf{E}_0^L\, \mathrm{e}^{ik_{Lz}d_L} \frac{\mathrm{e}^{ik_L z_L}}{i\lambda_L f} e^{\frac{ik_L}{2f}(x_L^2+y_L^2)} \iint_{-\infty}^{\infty} \mathrm{d}x\mathrm{d}y\, e^{i\mathbf{k}_L\mathbf{r}} e^{-\frac{ik_L}{f}(x_L x+y_L y)} \tag{2.48}$$

We need to evaluate the integral

$$I = \iint_{-\infty}^{\infty} \mathrm{d}x\mathrm{d}y\, e^{i\mathbf{k}_L\mathbf{r}} e^{-\frac{ik_L}{f}(x_L x+y_L y)} \tag{2.49}$$

Substituting $\mathbf{k}_L$ from equations (2.45) - (2.47) we receive

$$\begin{aligned} I &= \iint_{-\infty}^{\infty} \mathrm{d}x\mathrm{d}y\, e^{ik_L(\sin\theta\cos\xi x+\sin\theta\sin\xi y)} e^{-ik_L\left(\frac{x_L}{f}x+\frac{y_L}{f}y\right)} \\ &= \iint_{-\infty}^{\infty} \mathrm{d}x\mathrm{d}y\, e^{i2\pi(\nu_x x+\nu_y y)} \end{aligned} \tag{2.50}$$

where

$$\nu_x = \frac{1}{\lambda_L}\left(\sin\theta\cos\xi - \frac{x_L}{f}\right) \tag{2.51}$$

$$\nu_y = \frac{1}{\lambda_L}\left(\sin\theta\sin\xi - \frac{y_L}{f}\right) \tag{2.52}$$

are the spatial frequencies of the field being transformed. Now we can perform the integration

$$\begin{aligned} I &= \iint_{-\infty}^{\infty} \mathrm{d}x\mathrm{d}y\, e^{i2\pi(\nu_x x+\nu_y y)} = \int_{-\infty}^{\infty} \mathrm{d}x\, e^{i2\pi\nu_x x} \int_{-\infty}^{\infty} \mathrm{d}y\, e^{i2\pi\nu_y y} \\ &= \delta(\nu_x)\delta(\nu_y) \end{aligned} \tag{2.53}$$

where $\delta(\nu_x), \delta(\nu_y)$ are the Dirac δ-functions. Symbolically, we can rewrite the electric field (2.48)

$$\mathbf{E}_L(x_L, y_L) = \mathbf{E}_0^L\, \mathrm{e}^{ik_{Lz}d_L} \frac{\mathrm{e}^{ik_L z_L}}{i\lambda_L f} e^{\frac{ik_L}{2f}(x_L^2+y_L^2)} \delta(\nu_x)\delta(\nu_y) \tag{2.54}$$

Here we can see what was already mentioned, namely that the lens is a Fourier processor, which transforms an incident plane wave to the δ-function in the focal plane. This corresponds to the intuitive idea that the image of a plane wave is a single point in the focal plane.

2.4.4 Circular lens

A realistic lens is always finite and usually has a circular shape. Lets have such a lens of radius R and focal length f. In this case the transmissivity function is

$$t(x,y) = \begin{array}{ll} 1 & \text{for } \sqrt{x^2+y^2} < R \\ 0 & \text{elsewhere} \end{array}$$

In order to further simplify the task, we will calculate the distribution of electric field in the *focal plane*, i.e. we put $z_L = f$. For technical details of the calculation,

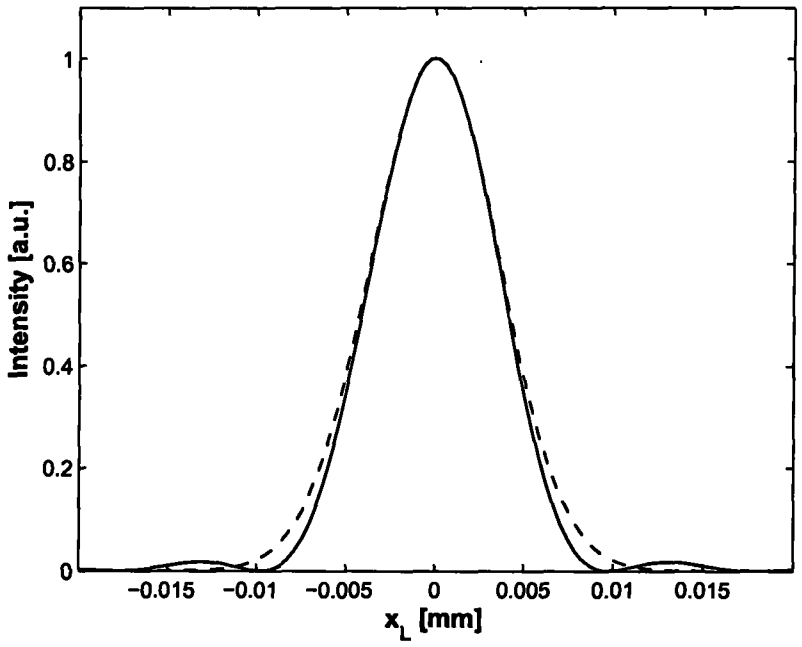

Figure 2.2: Intensity $\epsilon_0|\mathbf{E}_L|^2$ in the focal plane of a lens. Solid line corresponds to the lens with realistic aperture, Eq. (2.55), dashed line to the gaussian approximation of the aperture, Eq. (2.58). The incident wave is orthogonal to the lens. Used parameters are: lens radius $R = 2.5$ cm, focal length $f = 0.5$ m, and wave length $\lambda = 800$ nm.

see [10, p. 63]. Finally we have

$$\mathbf{E}_L(x_L, y_L) = \mathrm{E}_0^L \frac{e^{i(k_L f + k_{Lz} d_L)}}{i\lambda_L f} e^{i\frac{k_L}{2f}(x_L^2 + y_L^2)} 2\pi R \frac{J_1(\rho R)}{\rho} \tag{2.55}$$

where d_L is a distance between light source and lens, J_1 is Bessel function of the first kind and ρ is the quantity resulting from substitution of variables

$$\rho = \sqrt{\nu_x^2 + \nu_y^2} \;\; ; \;\; \begin{aligned} \nu_x &= k_{Lx} - \frac{k_L}{f} x_L \\ \nu_y &= k_{Ly} - \frac{k_L}{f} y_L \end{aligned}$$

As one can see in *Figure 2.2*, the intensity $\epsilon_0|\mathbf{E}_L|^2$ has its maximum at the position of the maximum of idealistic lens. The intensity quickly decreases as one leaves the position of maximum. There are also satellite maxima.

2.4.5 Gaussian lens

Exact treatment of Bessel function in multiple integral in the correlator would be possible on cost of extremely demanding numerical calculations. If one sacrifice the satellite maxima, it is possible to introduce a very simple approximation. To this end we replace sharp edges of the aperture by a smooth profile. With respect to the imaging properties of a lens and its shape, a good choice is the gaussian aperture

$$t(x,y) = e^{-\frac{x^2+y^2}{\sigma^2}} \tag{2.56}$$

Here, σ is a parameter of a gaussian, which is related with the full width at half of maximum (FWHM) by relationship

$$\sigma = \frac{FWHM}{2\sqrt{ln\,2}} \tag{2.57}$$

Similarly to the previous section, consider an incident electric field to be a monochromatic plane wave. When substituting to the diffraction integral, we can directly figure up the field behind a lens. After a straightforward calculation we obtain

$$\mathbf{E}_L(x_L,y_L) = \mathbf{E}_0^L \frac{\pi}{a} \frac{e^{i(k_L z_L + k_{Lz} d_L)}}{i\lambda_L z_L} e^{c_x - \frac{b_x^2}{4a}} e^{c_y - \frac{b_y^2}{4a}} \tag{2.58}$$

where

$$\begin{aligned} a &= -\frac{1}{\sigma^2} + i\frac{k_L}{2}\left(\frac{1}{z_L} - \frac{1}{f}\right) \\ b_x &= i\left(k_{Lx} - \frac{k_L}{z_L}x_L\right) \\ c_x &= i\frac{k_L}{2z_L}x_L^2 \\ b_y &= i\left(k_{Ly} - \frac{k_L}{z_L}y_L\right) \\ c_y &= i\frac{k_L}{2z_L}y_L^2 \end{aligned} \tag{2.59}$$

The obvious question which now appears is how are the two approaches to the lens aperture different, i.e. what is the difference between circular and gaussian lens. In order to compare these two descriptions, we made a simple estimate $\sigma = R/\sqrt{2}$.In *Figure 2.2*, the approximative intensity $\mathbf{EE}^*$ with $\mathbf{E}$ from (2.58) is compared with exact value given by (2.55). We can deduce following conclusions from *Figure 2.2*:

As we have expected, the gaussian profile of transmissivity does not lead to satellite maxima. These are caused by diffraction on sharp edges of the circular aperture, which we have removed by the use of the gaussian transmissivity with a smooth profile. The intensity of these oscillations is however, compared to the main maximum, negligible. We can also see, that both curves nearly match (we don't mean the small oscillations, but the main maximum of Bessel function). We note, that more sophisticated choice of parameters σ and transmissivity amplitude is possible. The simple choice $\sigma = R/\sqrt{2}$ is sufficient for our purpose.

It's also worth to notice a scale, i.e. how large is actually the maximum. The width of maximum is imponderable compared to the expected extent of a detector (of the order of 1 mm). It nicely corresponds to the intuitive idea, that the image of an incident monochromatic plane wave is a "point" in the focal plane of a lens.

It is important to emphasize, that in contrast to the relation (2.55) which is valid *exclusively* in the focal plane, the expression (2.58) remains valid for a general distance z_L behind the lens.

Finally we can state, that if we neglect diffraction pattern resulting from the diffraction on sharp edge of a circular aperture, a gaussian lens is a good approximation to the real lens.

2.5 Double slit

An important element in our experiment is the *double slit*. Although known at least since Young's famous experiment, it remains a useful device in today's physics. Though the principle of double slit is quite easy, the description of its functioning may differ depending on our needs. Lets have a look at some of these.

2.5.1 Hairlike double slit

Following the introductory paragraph of this chapter let us consider an ideal point double slit (hairlike double slit) perpendicular to the z axis sweeping with a plane $z = 0$. The distance between the slits is a. A *hairlike double slit* means that we take the y extent of each slit to be infinity and the x extent go towards zero. When investigating the field distribution behind a single slit, one can see, that the field has the *cylindrical* symmetry, where y is the axis of symmetry.

Field distribution behind a slit
This problem is also a standard one and it is solved in a number of textbooks, e.g. [11, p. 150]. For a better understanding of the problem, we repeat the most important steps. Consider a wave equation in the form

$$\left(\Delta - \frac{1}{c^2}\frac{\partial^2}{\partial t^2}\right)\mathbf{E}(\mathbf{r},t) = 0 \tag{2.60}$$

where c is the velocity of light. The Laplacian in the cylindrical coordinate system is

$$\Delta = \frac{\partial^2}{\partial r^2} + \frac{1}{r}\frac{\partial}{\partial r} + \frac{\partial^2}{\partial y^2} \tag{2.61}$$

where $r = \sqrt{x^2 + z^2}$ is the distance from a slit. Next we assume that we can separate the space and time component of electric field

$$E(r,y,t) = Q(r,y)e^{-i\omega t} \tag{2.62}$$

and moreover we suppose that we can use the *separation of variables* method in the space domain

$$Q(r,y) = u(r)w(y) \tag{2.63}$$

The wave equation then becomes

$$\frac{\partial^2 w}{\partial r^2}u + \frac{1}{r}\frac{\partial w}{\partial r}u + \frac{\partial^2 u}{\partial y^2}w + k^2 uw = 0$$

which we can separate into two parts, each depending on different variable and both must equal the same constant which we denote as q^2

$$-\frac{1}{u}\frac{\partial^2 u}{\partial y^2} = \frac{1}{w}\frac{\partial^2 w}{\partial r^2} + \frac{1}{rw}\frac{\partial w}{\partial r} + k^2 = q^2 \tag{2.64}$$

So we have a set of two differential equations

$$\frac{\partial^2 u}{\partial y^2} + q^2 u = 0 \tag{2.65}$$

$$\frac{\partial^2 w}{\partial r^2} + \frac{1}{r}\frac{\partial w}{\partial r} + p^2 w = 0 \tag{2.66}$$

where $p^2 = k^2 - q^2$. The solutions are

$$u(y) = e^{\pm iqy} \tag{2.67}$$

$$w(r) = CB(pr) \tag{2.68}$$

where C is a constant and B is some function from the class of Bessel functions. Namely, B can be one of the following functions: Bessel function of the first kind (J_0), Neumann function (N_0) or Hankel function (H_0), last named being of 1st or 2nd kind.

Further we demand, that our solution becomes a cylindrical wave

$$\mathbf{E}(r) = \frac{\mathbf{E}_0}{\sqrt{r}} e^{ikr} \tag{2.69}$$

for a large distance r from the slit. This is a property of both Hankel functions , but not of Bessel and Neumann functions.

If we realize again the symmetry of problem, we find out, that the electric field cannot be dependent on y because of the infinite extent of the slit and all points in the y direction are equal. So q is identically zero $q = 0$ and the space component of electric field (2.63) is thus

$$Q(r, y) = CH_0^1(kr)$$

Finding out the constant C is relatively easy. We require that the asymptotic expansion of Hankel function [12, p. 364]

$$H_0^1(kr) \approx \sqrt{\frac{2}{\pi kr}}\, e^{i(kr-\pi/4)}$$

merge with cylindrical wave (2.69). Omitting constant factor $\sqrt{\frac{\pi}{2}}\, e^{i\frac{\pi}{4}}$ we find

$$C = \sqrt{k}\mathbf{E}_0 \tag{2.70}$$

so that

$$\mathbf{E}(r, y) = \sqrt{k}\mathbf{E}_0 H_0^1(kr) \tag{2.71}$$

Interference at double slit

Likewise in the section (2.4) we will index all variables related to the double slit with letter S. With respect to the cylindrical symmetry we can reduce our 3D problem to the 2D one when confining to the plane $y_S = 0$. We consider (as well as in 2.4.3) a monochromatic plane wave incident in a general direction to the double slit. Let us entitle the slit of coordinates $\left[\frac{a}{2}, 0, 0\right]$ as slit I and the slit of coordinates $\left[-\frac{a}{2}, 0, 0\right]$ as slit 2. The detector is placed in the point $[x_S, 0, z_S]$ in the plane parallel to the double slit. Hence we can define the distances of each slit from the detector as

$$l_1 = \sqrt{\left(x_S - \frac{a}{2}\right)^2 + z_S^2} \tag{2.72}$$

$$l_2 = \sqrt{\left(x_S + \frac{a}{2}\right)^2 + z_S^2} \tag{2.73}$$

Next we need to express the phase shift φ of the field in slit 1 against slit 2. This is proportional to the projection of $\mathbf{k}_S$ vector to the x_S axis, which leads to

$$\varphi = ak_{Sx} \tag{2.74}$$

According to the principle of superposition, the field at detector is the sum of fields from both slits. With help of the result from previous section, the field at detector reads

$$\mathbf{E}_S(\mathbf{r}_S) = \mathbf{E}_S^1 + \mathbf{E}_S^2 = \sqrt{k_S}\mathbf{E}_0^S \left(e^{i\varphi} H_0^1(k_S l_1) + H_0^1(k_S l_2)\right) \tag{2.75}$$

The intensity profile for an orthogonally incident plane wave is shown in *Figure 2.3.*

2.5.2 Rectangular double slit

Consider now a realistic double slit, i.e. the double slit where both slits have the same rectangular shape. We also assume one extent of the rectangle to be considerably larger than the other. In accordance with the ideal hairlike double slit, we put the center of our coordinate system between the two rectangular slits in such way, that the longer side (length) of a slit is parallel to y axis and the width is

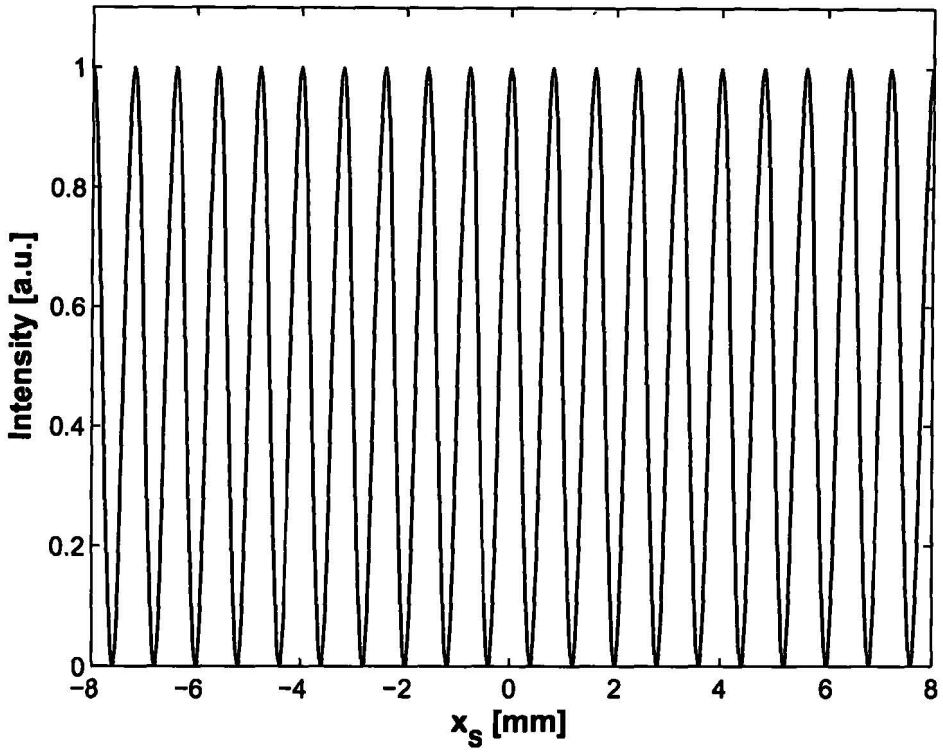

Figure 2.3: Intensity behind the hairlike double slit at distance $z_S = 1$ m. The distance between slits is $a = 1$ mm and the wave length $\lambda = 800$ nm

parallel to x axis. We then denote the width as l_x and the length as l_y. The distance between slits is a. It is evident, that the transmissivity is

$$t(x,y) = t_1(x,y) + t_2(x,y) \tag{2.76}$$

where

$$\begin{aligned} t_1(x,y) &= 1 \text{ for } \frac{a}{2} - \frac{l_x}{2} < x < \frac{a}{2} + \frac{l_x}{2}; \quad -\frac{l_y}{2} < y < \frac{l_y}{2} \\ &= 0 \text{ elsewhere} \end{aligned} \tag{2.77}$$

$$\begin{aligned} t_2(x,y) &= 1 \text{ for } -\frac{a}{2} - \frac{l_x}{2} < x < -\frac{a}{2} + \frac{l_x}{2}; \quad -\frac{l_y}{2} < y < \frac{l_y}{2} \\ &= 0 \text{ elsewhere} \end{aligned} \tag{2.78}$$

Substituting the rectangular transmissivity to the diffraction integral (2.34) would yield the analytical result ([10, p. 71]). However, the result would have a form

of Fresnel integrals like functions and thus would be quite uncomfortable for further manipulations. Because of this reason, we even wouldn't present this analytical result here. Instead of it, we try to find some other appropriate model which would facilitate the calculation of correlator keeping the major properties of a realistic rectangular double slit. Similarly to the section 2.4 we will consider a double slit with gaussian transmissivity.

2.5.3 Gaussian double slit

In this section we will try to figure out the properties of a gaussian double slit and compare it to the rectangular double slit. The transmissivity of each gaussian slit can be written in the form

$$t(x,y) = e^{-\frac{(x-x_c)^2}{\sigma_x^2} - \frac{(y-y_c)^2}{\sigma_y^2}} \tag{2.79}$$

where $[x_c, y_c]$ are coordinates of the center of a slit and σ_x, σ_y are parameters of the gaussian. After evaluating the diffraction integral (2.34), we can express the field distribution behind a slit as

$$\mathbf{E}_S(x_S, y_S) = \mathbf{E}_0^S \frac{e^{i(k_S z_S + k_{Sz} d_S)}}{i\lambda_S z_S} \frac{\pi}{\sqrt{a_x a_y}} e^{c_x - \frac{b_x^2}{4a_x}} e^{c_y - \frac{b_y^2}{4a_y}} \tag{2.80}$$

where d_S is a distance between light source and the plane of a slit (i.e. double slit) and

$$\begin{aligned}
a_x &= -\frac{1}{\sigma_x^2} + i\frac{k_S}{2z_S} \\
a_y &= -\frac{1}{\sigma_y^2} + i\frac{k_S}{2z_S} \\
b_x &= \frac{2x_c}{\sigma_x^2} + i\left(k_{Sx} - \frac{k_S}{z_S}x_S\right) \\
c_x &= -\frac{x_c^2}{\sigma_x^2} + i\frac{k_S}{2z_S}x_S^2 \\
b_y &= \frac{2y_c}{\sigma_y^2} + i\left(k_{Sy} - \frac{k_S}{z_S}y_S\right) \\
c_y &= -\frac{y_c^2}{\sigma_y^2} + i\frac{k_S}{2z_S}y_S^2
\end{aligned} \tag{2.81}$$

For simplicity, we will investigate the field in the plane $y_S = 0$. From the form of diffraction integral and the transmissivity function, one can see that both are

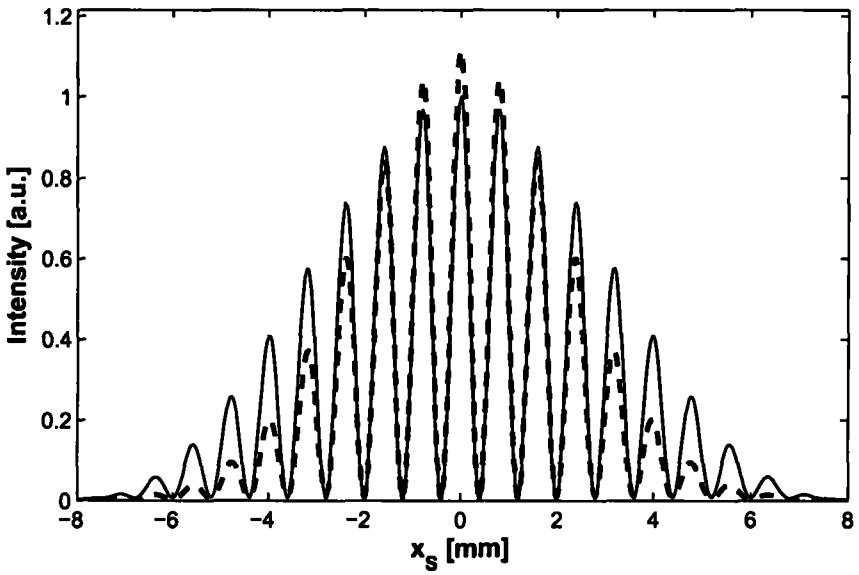

Figure 2.4: Intensity behind the double slit at distance $z_S = 1$ m. Solid line corresponds to the rectangular double slit (realistic model), dashed line to the gaussian double slit (approximative model). Incident wave is orthogonal, $a = 1$ mm, $l_x = 0.1$ mm, and $\lambda = 800$ nm.

separable into the x and y components. In other words if we are interested in the area where $y = constant$, we don't need to evaluate integration over y, because it contributes to the result only by a constant factor.

A situation for both rectangular and gaussian double slit is shown in *Figure 2.4*. We can see a good agreement of both interference patterns. If we chose the parameters of gaussian (σ and transmissivity amplitude, which we take to be 1) more carefully we would be able to find a perfect match of both intensities. We can say, that the approximation by a gaussian double slit is a good approach.

Spot also the difference between *Figure 2.4* and *Figure 2.3*. The idealistic model of hairlike double slit describes well the periodicity of interference pattern, but doesn't involve the decay of intensity at the edges of the pattern as it is obvious from the above figures.

Chapter 3

Two-photon correlator

Now we discuss the principle of the whole experiment in more detail. After the generation of an entangled photon pair, into the path of one of photons we put a lens which causes the Fourier transform and creates image of an incident field. To the path of the other photon we place a double slit. The important thing is, that till the moment of measurement, i.e. detection of signals with detectors D_L and D_S, both photons exist in a superposition of possible quantum states described by state vector (2.27). Consider ideal point detectors in both branches of our experiment. The detector D_L is placed behind a lens, the other detector D_S is placed behind a double slit. Usually we would fix the position of one detector and measure the field distribution using the other detector. The question is how will look the correlator of such an experiment.

Our aim is to calculate correlator (2.11)

$$G_I(\mathbf{r}_L, t_L, \mathbf{r}_S, t_S) = \left\langle \mathbf{E}_L^{(-)}(\mathbf{r}_L, t_L)\mathbf{E}_S^{(-)}(\mathbf{r}_S, t_S)\mathbf{E}_S^{(+)}(\mathbf{r}_S, t_S)\mathbf{E}_L^{(+)}(\mathbf{r}_L, t_L)\right\rangle$$

We will evaluate the correlator with the help of state vector (2.27)

$$|\psi\rangle = \int\int \mathrm{d}\mathbf{k}_L \mathrm{d}\mathbf{k}_S \, F \, a^\dagger_{\mathbf{k}_L} a^\dagger_{\mathbf{k}_S} |vac\rangle$$

All deductions made up to here for electric fields are valid also for both, classical or quantum fields. Space components of $\mathbf{E}_L, \mathbf{E}_S$ are described by classical fields derived in previous sections. These relations describe the fields only for a single mode $\mathbf{k}_L$, $\mathbf{k}_S$ respectively. In a general case we have to integrate over the whole k-space to involve all possible modes. Using the definitions (2.3),(2.4) we can write our fields in the second quantization as

$$\begin{aligned}
\mathbf{E}_L^{(-)}(\mathbf{r}_L, t_L) &= \int \frac{\mathrm{d}\mathbf{k}_L^-}{(2\pi)^3}\, \mathbf{E}^*_{L,\mathbf{k}_L^-}(\mathbf{r}_L, t_L) a^\dagger_{\mathbf{k}_L^-} \\
\mathbf{E}_L^{(+)}(\mathbf{r}_L, t_L) &= \int \frac{\mathrm{d}\mathbf{k}_L^+}{(2\pi)^3}\, \mathbf{E}_{L,\mathbf{k}_L^+}(\mathbf{r}_L, t_L) a_{\mathbf{k}_L^+} \qquad (3.1) \\
\mathbf{E}_S^{(-)}(\mathbf{r}_S, t_S) &= \int \frac{\mathrm{d}\mathbf{k}_S^-}{(2\pi)^3}\, \mathbf{E}^*_{S,\mathbf{k}_S^-}(\mathbf{r}_S, t_S) a^\dagger_{\mathbf{k}_S^-} \\
\mathbf{E}_S^{(+)}(\mathbf{r}_S, t_S) &= \int \frac{\mathrm{d}\mathbf{k}_S^+}{(2\pi)^3}\, \mathbf{E}_{S,\mathbf{k}_S^+}(\mathbf{r}_S, t_S) a_{\mathbf{k}_S^+} \qquad (3.2)
\end{aligned}$$

where we indexed the modes respectively to the field they belong to. The time dependencies are described by equations (2.9), (2.10).

3.1 Order of field operators

We see, that as the indispensable part in the calculation of correlator we have to evaluate the action of all field operators on the vacuum state. We can further simplify our problem assuming, that the modes corresponding to the lens are well separated from those corresponding to the double slit. In other words, all L operators commute with all S operators. Hence we can write

$$\begin{aligned}&\left\langle \mathbf{E}_L^{(-)}\mathbf{E}_S^{(-)}\mathbf{E}_S^{(+)}\mathbf{E}_L^{(+)}\right\rangle \\ &\sim \int \mathrm{d}\tilde{\mathbf{k}}_L\mathrm{d}\tilde{\mathbf{k}}_S\mathrm{d}\mathbf{k}_L^-\mathrm{d}\mathbf{k}_S^-\mathrm{d}\mathbf{k}_L^+\mathrm{d}\mathbf{k}_S^+\mathrm{d}\mathbf{k}_L\mathrm{d}\mathbf{k}_S \left\langle a_{\tilde{\mathbf{k}}_L}a_{\tilde{\mathbf{k}}_S}a^\dagger_{\mathbf{k}_L^-}a^\dagger_{\mathbf{k}_S^-}a_{\mathbf{k}_L^+}a_{\mathbf{k}_S^+}a^\dagger_{\mathbf{k}_L}a^\dagger_{\mathbf{k}_S}\right\rangle \end{aligned} \tag{3.3}$$

where

$$\left\langle a_{\tilde{\mathbf{k}}_L}a_{\tilde{\mathbf{k}}_S}a^\dagger_{\mathbf{k}_L^-}a^\dagger_{\mathbf{k}_S^-}a_{\mathbf{k}_L^+}a_{\mathbf{k}_S^+}a^\dagger_{\mathbf{k}_L}a^\dagger_{\mathbf{k}_S}\right\rangle = \delta_{\tilde{\mathbf{k}}_L\mathbf{k}_L^-}\delta_{\tilde{\mathbf{k}}_S\mathbf{k}_S^-}\delta_{\mathbf{k}_L^+\mathbf{k}_L}\delta_{\mathbf{k}_S^+\mathbf{k}_S} \tag{3.4}$$

Our correlator then becomes

$$\begin{aligned}G_I(\mathbf{r}_L,t_L,\mathbf{r}_S,t_S) &= \int \mathrm{d}\tilde{\mathbf{k}}_L\mathrm{d}\tilde{\mathbf{k}}_S F^*(\tilde{\mathbf{k}}_L,\tilde{\mathbf{k}}_S)\mathbf{E}^*_{L,\tilde{\mathbf{k}}_L}(\mathbf{r}_L,t_L)\mathbf{E}^*_{S,\tilde{\mathbf{k}}_S}(\mathbf{r}_S,t_S)\cdot \\ &\times \int \mathrm{d}\mathbf{k}_L\mathrm{d}\mathbf{k}_S F(\mathbf{k}_L,\mathbf{k}_S)\mathbf{E}_{L,\mathbf{k}_L}(\mathbf{r}_L,t_L)\mathbf{E}_{S,\mathbf{k}_S}(\mathbf{r}_S,t_S)\end{aligned} \tag{3.5}$$

so we have two independent 6-dimensional integrations. Note also, that the field $\mathbf{E}_S$ is in fact the sum of fields from each slit, i.e.

$$\mathbf{E}_S = \mathbf{E}_S^1 + \mathbf{E}_S^2$$

thus we have actually four instead of two integrations. It is sufficient to calculate the part of integrand corresponding to the first slit $F\,\mathbf{E}_L\,\mathbf{E}_S^1$. The calculation of the part for the second slit is totally analogous. For this reason we introduce a notation g_1 for the part of correlator corresponding to the first slit and g_2 for the second slit, so that we can write for the correlator

$$G_I = (g_1+g_2)^*(g_1+g_2) \tag{3.6}$$

where

$$g_i = \int \mathrm{d}\mathbf{k}_L\mathrm{d}\mathbf{k}_S F\,\mathbf{E}_L\mathbf{E}_S^i \;; \qquad i=1,2$$

The factor (g_1+g_2) corresponds to the second integration in (3.5), $(g_1+g_2)^*$ to the first one.

3.2 Choice of coordinate system and momentum conservation

A technical detail is the choice of coordinate system. Consider a situation shown in *Figure 1.2.* Note that because of the law of momentum conservation discussed in section 2.2 and of geometry of our experiment in which the pump laser beam is orthogonally incident to the crystal, all three vectors $\mathbf{k_0}$, $\mathbf{k}_L$ and $\mathbf{k}_S$ lie in the same plane. We put this plane to be $y = 0$. Three coordinate systems were introduced in order to describe our experiment. They are related to crystal (position vector (x, y, z)), lens (position vector (x_L, y, z_L)) and double slit (position vector (x_S, y, z_S)). For technical needs of calculation, it is useful to specify transformations from one coordinate system to the other coordinate systems. Helpful relations are the transformation from the crystal coordinate system

$$\begin{pmatrix} x_L \\ z_L \end{pmatrix} = \begin{pmatrix} \cos\alpha & -\sin\alpha \\ \sin\alpha & \cos\alpha \end{pmatrix} \begin{pmatrix} x \\ z \end{pmatrix} \tag{3.7}$$

and

$$\begin{pmatrix} x_S \\ z_S \end{pmatrix} = \begin{pmatrix} \cos\beta & \sin\beta \\ -\sin\beta & \cos\beta \end{pmatrix} \begin{pmatrix} x \\ z \end{pmatrix} \tag{3.8}$$

and vice-versa, the transformation to the crystal coordinate system

$$\begin{pmatrix} x \\ z \end{pmatrix} = \begin{pmatrix} \cos\alpha & \sin\alpha \\ -\sin\alpha & \cos\alpha \end{pmatrix} \begin{pmatrix} x_L \\ z_L \end{pmatrix} \tag{3.9}$$

and

$$\begin{pmatrix} x \\ z \end{pmatrix} = \begin{pmatrix} \cos\beta & -\sin\beta \\ \sin\beta & \cos\beta \end{pmatrix} \begin{pmatrix} x_S \\ z_S \end{pmatrix} \tag{3.10}$$

The directions α and β (which we take to be fixed in our model) aren't nevertheless chosen haphazardly.
Lets denote the wave vectors corresponding to directions α, β as $\mathbf{k}_a$,$\mathbf{k}_b$. The vectors are constant vectors for some concrete parameters of our experiment, i.e. we don't integrate over those vectors.

We assume the phase matching of the first kind is satisfied, i.e. $\mathbf{k_0}$ respects the extraordinary (n_e) and $\mathbf{k}_a$, $\mathbf{k}_b$ the ordinary (n_o) refraction index. We can then rewrite the energy and momentum conservation laws, described by set of equations (2.12),(2.15),(2.16) to the form

$$\frac{n_o}{n_e}k_0 = k_a + k_b \tag{3.11}$$

$$k_a \sin\alpha = k_b \sin\beta \tag{3.12}$$

$$k_a \cos\alpha + k_b \cos\beta = k_0 \tag{3.13}$$

which is a set of three equations for four variables. If we choose one variable as our input parameter, the others are determined.

3.3 Correlator of simple ideal model

In our idealistic model we consider the infinite non-linear crystal, pump beam in a form of plane wave, lens with infinite aperture, a hairlike double slit and ideal point detectors.
Following the procedure from previous section, we will calculate the part g_1 of correlator. Substituting F, $\mathbf{E}_L$ and $\mathbf{E}_S^1$ by equations (2.28), (2.54) and (2.75) we obtain

$$\begin{aligned} g_1 &= C \int \mathrm{d}\mathbf{k}_L \mathrm{d}\mathbf{k}_S \delta(\mathbf{k}_0 - \mathbf{k}_L - \mathbf{k}_S)\delta(\omega_0 - \omega_L - \omega_S)\delta(\nu_x)\delta(\nu_y) \\ &\quad \times \frac{1}{\lambda_L f} e^{i\frac{k_L}{2f}(x_L^2+y_L^2)} \sqrt{k_S}\, e^{iak_{S_x}} H_0^1(k_S l_1) \end{aligned} \tag{3.14}$$

where C is a constant factor involving all parts which don't participate in integration, the first two δ-functions represent the momentum and energy conservation laws. For ν_x, ν_y in the last two δ-functions we write (see relations (2.51) and (2.52))

$$\nu_x = \frac{1}{\lambda_L f}(f \sin\theta \cos\xi - x_L) \tag{3.15}$$

$$\nu_y = \frac{1}{\lambda_L f}(f \sin\theta \sin\xi - y_L) \tag{3.16}$$

Due to energy and momentum conservation laws, we get rid of integration over $\mathbf{k}_S$. We can express the remaining itegration over $\mathbf{k}_L$ in spherical coordinates

$$\int \mathrm{d}\mathbf{k}_L = \int \mathrm{d}k_L \mathrm{d}\theta \mathrm{d}\xi\, k_L^2 \sin\theta \tag{3.17}$$

The position of detector D_L behind the lens is directly connected to the detected mode as it is obvious from relations for ν_x, ν_y. Putting the detector to the position $[x_L, y_L]$ we choose the k-vector with direction described by angles θ, ξ (see (2.45), (2.46)). This assignment is unique. Referring to section 2.2 it also implies, that value of k_L consistent with conservation laws (2.15), (2.16) and (2.12) depends on the position of detector D_L. However it is not our goal to describe the idealistic model in all details, so we won't present the calculation showing the dependence of k_L on $[x_L, y_L]$.
To distinguish the value of k_L corresponding to the position of detector D_L from the integration variable k_L lets denote the first one as K_L, where

$$K_L = K_L(x_L, y_L)$$

Repeat again, that due to energy and momentum conservation laws, we got rid of all integrations except the integration over θ and ξ. To find the part of correlator g_1, we will perform next manipulations.

To clarify the meaning of k_{Sx}, we will express it in more explicit form. Firstly, note, that k_{Sx} is the x-component of vector k_S in the double slit coordinate system. To show its dependence on K_L, we express this quantity in the crystal coordinate system using the transformation (3.10). With the help of momentum conservation law we have

$$\begin{aligned} k_{Sx} &= K_L \sin\gamma\cos\beta + (k_0 - K_L\cos\gamma)\sin\beta \\ &= K_L \sin(\gamma-\beta) + k_0 \sin\beta \end{aligned} \tag{3.18}$$

where γ, given by $\gamma = \alpha + \kappa$, is the angle between the projection of $\mathbf{K}_L$ to the $x-z$ plane and a pump beam $\mathbf{k}_0$. The angle κ satisfies

$$\tan\kappa = \tan\theta\cos\xi$$

Next, we express the value of k_S using the energy conservation law

$$k_S = k_0\frac{n_o}{n_e} - K_L \tag{3.19}$$

Finally, we would like to evaluate the action of $\delta(\nu_x,\nu_y)$, for which we write

$$\begin{aligned} \delta(\nu_x,\nu_y) &= (\lambda_L f)^2\delta\left(f\sin\theta\cos\xi - x_L, f\sin\theta\sin\xi - y_L\right) \\ &= (\lambda_L f)^2\delta\left(X - x_L, Y - y_L\right) \end{aligned} \tag{3.20}$$

where we introduced a substitution

$$\begin{aligned} X &= f\sin\theta\cos\xi \\ Y &= f\sin\theta\sin\xi \end{aligned}$$

with Jacobian J

$$J = f^2\sin\theta\cos\theta$$

Our integration over angles then becomes

$$\int \mathrm{d}\theta\mathrm{d}\xi\ \sin\theta\,(\lambda_L f)^2\, e^{iak_{Sx}}\delta(\nu_x,\nu_y) =$$

$$\begin{aligned} &= \int \mathrm{d}\theta\mathrm{d}\xi\, f^2\sin\theta\cos\theta\,\frac{\lambda_L^2}{\cos\theta}\, e^{iaK_L\sin(\gamma(\theta,\xi)-\beta)}\,\delta(X - x_L, Y - y_L) \\ &= \int \mathrm{d}X\mathrm{d}Y\,\frac{\lambda_L^2}{\sqrt{1-\frac{X^2+Y^2}{f^2}}}\, e^{iaK_L\sin(\gamma(X,Y)-\beta)}\,\delta(X - x_L, Y - y_L) \\ &= \frac{\lambda_L^2}{\sqrt{1-\frac{x_L^2+y_L^2}{f^2}}}\, e^{iaK_L\sin(\gamma(x_L,y_L)-\beta)} \end{aligned} \tag{3.21}$$

Putting all operations together yields the resulting form of g_1

$$g_1 = \tilde{C}\frac{1}{f\sqrt{1-\frac{x_L^2+y_L^2}{f^2}}}K_L e^{i\frac{K_L}{2f}(x_L^2+y_L^2)} \times \sqrt{k_0\frac{n_o}{n_e}-K_L}\; e^{iaK_L\sin(\gamma(x_L,y_L)-\beta)}e^{iak_0\sin\beta}\,H_0^1\left(\left[k_0\frac{n_o}{n_e}-K_L\right]l_1\right) \quad (3.22)$$

where $\tilde{C}$ is a constant factor, a is the distance between slits and l_1 is described by relation (2.72). Calculation of g_2 is analogous.

We are now completely able to calculate the correlator of idealistic model.

3.4 Correlator in a realistic approximation

In this section we will calculate the correlator (2.11) of our realistic approximation, i.e. the model with finite crystal, gaussian pump beam, gaussian lens and gaussian double slit. We still assume the use of ideal detectors, which are point-like and infinitely fast.

3.4.1 Integrand

Note, that we integrate over the whole k-space. Such integration would be quite easy and would provide us with analytical result if the integrand had been of the form of a gaussian. One can guess, that this choice isn't heuristic. It is motivated not only by the need of easy integration, but also by the resemblance of the gaussian with other functions we deal with and which are a part of the integration. Similarly to the sections 2.4.5 and 2.5.3 we will try to replace the functions similar to gaussian with the gaussian.
After having evaluated the action of operators to the vacuum state, lets have a look at the form of integrand itself. For an example, we take the first integrand from our two 6D integrations in (3.5). Later on, we will also show, that the second integration is simply the complex conjugate of the first one.

We can substitute F, $\mathbf{E}_L$, $\mathbf{E}_S$ from equations (2.28), (2.58), (2.80). The time dependencies of electric fields are given by (2.9). The whole expression is relatively complicated so we won't write it here in all details. We rather separate it schematically to individual components and we will describe the used techniques of calculation for those components. Our integrand now reads

$$\begin{aligned} F\mathbf{E}_L\mathbf{E}_S^1 \;=\; & C\,\frac{\sin\left[\frac{1}{2}(\omega_0-\omega_L-\omega_S)\tau\right]}{\frac{1}{2}(\omega_0-\omega_L-\omega_S)}\,\frac{\sin\left[\frac{1}{2}(\mathbf{k}_0-\mathbf{k}_{Lz}-\mathbf{k}_{Sz}-K)l\right]}{\frac{1}{2}(\mathbf{k}_0-\mathbf{k}_{Lz}-\mathbf{k}_{Sz}-K)} \\ & \times h(\mathbf{k}_L,\mathbf{k}_S)e^{-i(\omega_L t_L+\omega_S t_S)}\,e^{A(\mathbf{k}_L,\mathbf{k}_S)+iB(\mathbf{k}_L,\mathbf{k}_S)} \end{aligned} \tag{3.23}$$

where we expressively left the sinc like functions. In the following text we explain the meaning of each factor.

C is a factor which includes all components of F, $\mathbf{E}_L$ and $\mathbf{E}_S^1$ which do not dependend on $\mathbf{k}_L$ or $\mathbf{k}_S$ and thus do not take part in the integration.

Next we deal with sinc like functions, i.e. the functions of the form $\sin(ax)/x$, which is an oscillating function. Just those oscillations would make the calculation rather difficult. Accordingly to the introductory paragraph of this section, we will try to replace the sinc like functions by a gaussian. Assume a sinc like function $\sin(ax)/x$

and a gaussian ce^{-bx^2}, where x is variable and a, b, c are parameters. We demand a good agreement of both functions around their maximum. We thus demand their values in the maximum equal

$$ce^{-bx^2} = \frac{\sin(ax)}{x} \tag{3.24}$$

which is satisfied for

$$c = a \tag{3.25}$$

Next we demand the second derivations of both functions to equal, in other words the coefficients of the second order member in their series expansion equal.

$$\left(ae^{-bx^2}\right)'' = \left(\frac{\sin(ax)}{x}\right)'' \tag{3.26}$$

which gives

$$b = \frac{1}{6}a^2 \tag{3.27}$$

Finally we have

$$\frac{\sin(ax)}{x} \approx ae^{-\frac{1}{6}a^2x^2} \tag{3.28}$$

The behaviour of both functions in (3.28) is plotted in *Figure 3.1.* Our *sincs* in correlator become

$$\frac{\sin\left[\frac{1}{2}(\omega_0 - \omega_L - \omega_S)\tau\right]}{\frac{1}{2}(\omega_0 - \omega_L - \omega_S)} \approx \tau e^{-\frac{\tau^2}{24}(\omega_0 - \omega_L - \omega_S)^2} \tag{3.29}$$

$$\frac{\sin\left[\frac{1}{2}(\mathbf{k}_0 - \mathbf{k}_{Lz} - \mathbf{k}_{Sz} - K)l\right]}{\frac{1}{2}(\mathbf{k}_0 - \mathbf{k}_{Lz} - \mathbf{k}_{Sz} - K)} \approx le^{-\frac{l^2}{24}(\mathbf{k}_0 - \mathbf{k}_{Lz} - \mathbf{k}_{Sz} - K)^2} \tag{3.30}$$

In order to transform the function h to its exponential form, we use a simple identity

$$h = e^{\ln(h)} \tag{3.31}$$

Let us discuss the time dependent factor $e^{-i(\omega_L t_L + \omega_S t_S)}$. As it can bee seen from the form of our state vector, the correlator is not averaged over the time. The value of our correlator is hence the value in some specific instant. Generally we can choice whichever time instant on both detectors, but evidently the most meaningful moment would be, when the maximum of generated wave packet impacts the detector. The time needed for propagation of the generated photon to the detector is then

$$t_i = \frac{\sqrt{x_i^2 + y_i^2 + (d_i + z_i)^2}}{c} n_o \; ; \qquad i = L, S \tag{3.32}$$

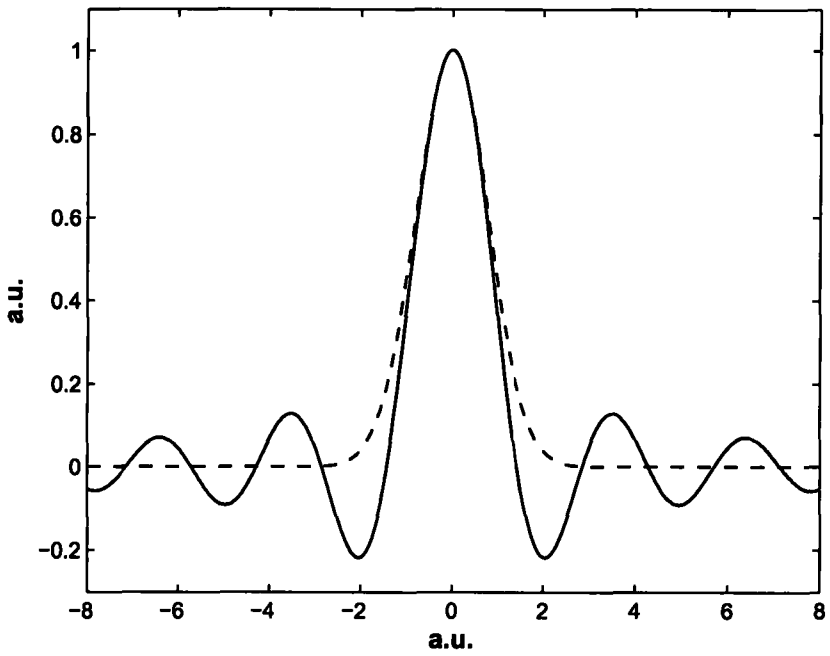

Figure 3.1: Comparison of sinc like vs. gaussian function. Solid line corresponds to the sinc like function (realistic model), dashed line to the gaussian function (approximative model).

where $[x_i, y_i]$ is the position of detector, c is the light velocity in vacuum and n_o is the refractive index of the media. The phase factors then become

$$\omega_i t_i = k_i \sqrt{x_i^2 + y_i^2 + (d_i + z_i)^2} \; ; \qquad i = L, S \tag{3.33}$$

This is true for the propagation in the free space (with refractive index n_o). The propagation of the beams in our system is however influenced by optical elements - the lens and the double slit. It means, that the time needed for propagation of the maximum of wave packet from the source to the detector is not exactly the time given by (3.32). But this imperfection will cause only the decrease of amplitude of interference pattern at the given point, and will not afflict the interference itself.

The last factor is already in the exponential form, where A is its real and B its imaginary part.
Using the above described relations, the integrand (3.23) now reads

$$F\mathbf{E}_L\mathbf{E}_S^1 = \tilde{C}e^{\tilde{A}(\mathbf{k}_L,\mathbf{k}_S)+i\tilde{B}(\mathbf{k}_L,\mathbf{k}_S)} \tag{3.34}$$

where $\tilde{C}$ is a new constant factor and $\tilde{A}$, $\tilde{B}$ are new real and imaginary part of the integrand. This is already the desired exponential form suitable for integration.

3.4.2 Method of calculation

Though the form (3.34) is already suitable for integration, we must discuss some more details. One of the main physical properties we want to involve in our theoretical model is the deviation from the exact phase matching. For a simplicity of our dialect we will call it (little incorrectly) deviations from the conservation laws. To do this, we define new vectors $\mathbf{\Delta}_L$, $\mathbf{\Delta}_S$ describing the deviations of $\mathbf{k}_L$, $\mathbf{k}_S$ from the energy and momentum conservation laws. We then write

$$\mathbf{k}_L = \mathbf{k}_a + \mathbf{\Delta}_L \tag{3.35}$$

$$\mathbf{k}_S = \mathbf{k}_b + \mathbf{\Delta}_S \tag{3.36}$$

In order to further simplify our task, we introduce a 6-dimensional vector $\mathbf{\Delta}$

$$\mathbf{\Delta} = \begin{pmatrix} \mathbf{\Delta}_L \\ \mathbf{\Delta}_S \end{pmatrix} = \begin{pmatrix} \Delta_{Lx} \\ \Delta_{Ly} \\ \Delta_{Lz} \\ \Delta_{Sx} \\ \Delta_{Sy} \\ \Delta_{Sz} \end{pmatrix} \tag{3.37}$$

The functions $\tilde{A}(\mathbf{k}_L, \mathbf{k}_S)$, $\tilde{B}(\mathbf{k}_L, \mathbf{k}_S)$ in the integrand (3.34) aren't the polynomials in $\mathbf{\Delta}$. The calculation would become quite comfortable if the integrand was in the form of a gaussian. Looking at $\mathbf{\Delta}$ as the perturbation from momentum conservation law, we can make a series expansion of $\tilde{A}$ and $\tilde{B}$ with precision of order $\mathbf{\Delta}^2$. This expansion is identical to the so-called saddle point approximation.

If doing so, our part of correlator

$$g_1 = \tilde{C} \int \mathrm{d}\mathbf{k}_L \mathrm{d}\mathbf{k}_S \, e^{\tilde{A}(\mathbf{k}_L, \mathbf{k}_S) + i\tilde{B}(\mathbf{k}_L, \mathbf{k}_S)} \tag{3.38}$$

becomes

$$g_1 = \tilde{C} \int \mathrm{d}\mathbf{\Delta} \, e^{\mathbf{\Delta} M \mathbf{\Delta} + \mathbf{v}\mathbf{\Delta} + D} \tag{3.39}$$

where the exponent of integrand is quadratic form in $\mathbf{\Delta}$: M is 6x6 coefficients matrix, $\mathbf{v}$ is 6-dimensional coefficients vector and D is a constant coefficient. Continuing in our considerations, we introduce a substitution $\mathbf{\Delta} = \mathbf{\Delta}' + \mathbf{\Delta}_0$. We now integrate over $\mathbf{\Delta}'$, i.e. $\mathrm{d}\mathbf{\Delta} \Rightarrow \mathrm{d}\mathbf{\Delta}'$. The exponent of integrand takes now a form

$$\mathbf{\Delta} M \mathbf{\Delta} + \mathbf{v}\mathbf{\Delta} + D = \mathbf{\Delta}' M \mathbf{\Delta}' + (2\mathbf{\Delta}_0 M + \mathbf{v})\mathbf{\Delta}' + \mathbf{\Delta}_0 M \mathbf{\Delta}_0 + \mathbf{v}\mathbf{\Delta}_0 + D \tag{3.40}$$

If we substitute $\mathbf{\Delta}_0 = -\frac{1}{2}\mathbf{v}M^{-1}$ to the exponent, we have

$$\mathbf{\Delta}'M\mathbf{\Delta}' + \frac{1}{2}\mathbf{v}\mathbf{\Delta}_0 + D$$

The part g_1 of correlator now reads

$$g_1 = \tilde{C}e^{-\frac{1}{4}\mathbf{v}M^{-1}\mathbf{v}+D}\int \mathrm{d}\mathbf{\Delta}'\, e^{\mathbf{\Delta}'M\mathbf{\Delta}'} \tag{3.41}$$

The result of integration is

$$\int \mathrm{d}\mathbf{\Delta}'\, e^{\mathbf{\Delta}'M\mathbf{\Delta}'} = \frac{\pi^3}{\sqrt{\det M}} \tag{3.42}$$

Finally, the relation for g_1 is

$$g_1 = \tilde{C}e^{-\frac{1}{4}\mathbf{v}M^{-1}\mathbf{v}+D}\,\frac{\pi^3}{\sqrt{\det M}} \tag{3.43}$$

As we can see, it is sufficient to know only M, $\mathbf{v}$ and D for the complete evaluation of the part of correlator g_1 . In our model, the form of M, $\mathbf{v}$ and D is always achievable, we do just the series expansion of functions $\tilde{A}$ and $\tilde{B}$. The calculation of the other part of correlator g_2 is assez analogous.

We can thus state, that we are now completely able to calculate the correlator in our realistic approximation.

Chapter 4

Comparison of the theory with experiment

In the previous chapter we have derived the correlator of simple ideal model in the analytical form. In principle we can write down all elements of matrix M, vector $\mathbf{v}$ and constant factor D and turn the formula (3.43) into an explicit expression, too. However, this expression is very complicated and we find it advantageous to discuss the realistic approximation directly from numerical results.

Both models, idealistic and approximative, depend on a relatively large number of parameters. The number of input parameters ranges from 11 for the simple ideal model up to 20 for the approximative model. Obviously, the most interesting features demonstrating the properties of entanglement will be the dependence of the correlator on the mutual position of detectors D_L and D_S. Our variables are then the position x_L of the detector D_L and the position x_S of the detector D_S. Values of the other parameters we used in our calculations are listed in *Table 4.1.*

The refractive indices correspond to the $LiIO_3$ crystal, which is commonly used in this type of experiment. Also other parameters arise from the real experiment, namely the phase matching of the first kind is used so that both signal and idler light beam have the same mean frequency and include the same angle with the pump beam, i.e., $\alpha = \beta$. For simplicity we assume no dispersion, which means, that all light beams originating in crystal during the process of down conversion respect the same ordinary refractive index n_o. Namely, the value of extraordinary refractive index is calculated for the pump wave length 405 nm and similarly, the value of ordinary refractive index corresponds to the wave length 810 nm, both in the air.

One has to keep in mind, that we take into account only the coincidental events. Note also, that our correlator (3.5) is not normalized. However, the physically interesting information lies in visibility of fringes, which are best represented in arbitrary units.

wave length of the pump beam in the air	λ_0	=	405 nm
extraordinary refractive index	n_e	=	1.7824
ordinary refractive index	n_o	=	1.8671
angle between the lens axis and the pump beam	β	=	17.3^o
width of the crystal	l	=	1 cm
time duration of the pump pulse	τ	=	330 ns
Rayleigh length of the pump beam	z_0	=	0.1 m
distance between the crystal and the lens	d_L	=	1 m
radius of the lens	R	=	3 cm
focal length	f	=	1 m
position $[x_L, y_L]$ of the detector D_L behind the lens	y_L	=	0 m
distance between the lens and the detection plane (unless specified, the detector D_L is in the focal plane)	z_L	=	1 m
distance between the crystal and the double slit	d_S	=	1 m
width of the slits	l_x	=	0.1 mm
length of the slits	l_y	=	5 cm
distance between the slits	a	=	0.7 mm
position $[x_S, y_S]$ of the detector D_S behind the lens	y_S	=	0 m
distance between the double slit and the detection plane	z_S	=	1 m

Table 4.1: Numerical values of used parameters

4.1 Simple ideal model

Lets start with easier ideal model involving infinite crystal, infinite lens and hairlike double slit. First, we consider the intuitively more comprehensible situation, where we fix our detector D_L in the focal length f behind the lens. The position of detector is fixed at x_L. We measure the signal behind the double slit as a function of position x_S of detector D_S. The dependence of interference pattern behind the double slit on the position of D_L is shown in *Figure 4.1*

The result is in good agreement with an intuitive expectation. By setting up a particular position x_L of detector behind the lens, we choose a single mode to which corresponds a conjugated single mode incident to the double slit. Since we monitor only close vicinity of the axis of the double slit, we obtain the perfect visibility of interference. Changing x_L, we change the wave vector incident on the double slit, which causes the shift of interference fringes. Notice the direction of this shift. The increasing position of x_L causes the shift of interference fringes also to higher values

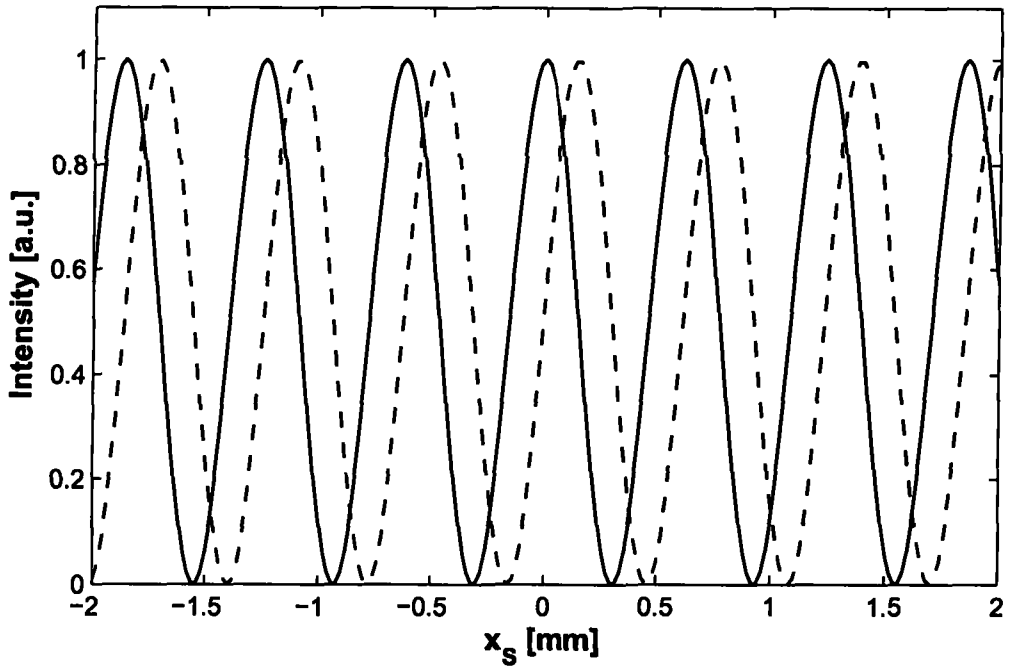

Figure 4.1: Simple ideal model: Interference pattern behind the double slit for different positions of D_L. Solid and dashed line correspond to the position of detector D_L behind the lens $x_L = 0$ and 0.15 mm.

of x_S. This corresponds exactly to the momentum conservation law (2.15-2.16), which states, that higher α_L is related to smaller α_S and vice-versa. Actually, this is not true for the whole interval $(0; \pi/2)$, but it is true for α_L and α_S around β, which is our case.

Now have a look at the other interesting and probably less intuitive set up. Here we fix the detector D_S behind the double slit and we detect the signal in the focal plane of the lens. The result is shown in *Figure 4.2.*

The field distribution behind the lens can be explained if we realize, that the detector D_S detects all possible modes, each contributing with different weight. Conjugated modes, which propagate to the lens, create the particular field distribution. For example, we fix the detector D_S in the position $x_S = 0$ mm. We make the first measurement behind the lens in the position $x_L = 0$ mm. We know, that in the focal plane, one concrete point corresponds more or less to one concrete wave vector. For example, our point $x_L = 0$ mm corresponds to the orthogonal incident wave vector. Namely, the mode impacting the double slit, which is conjugated to our

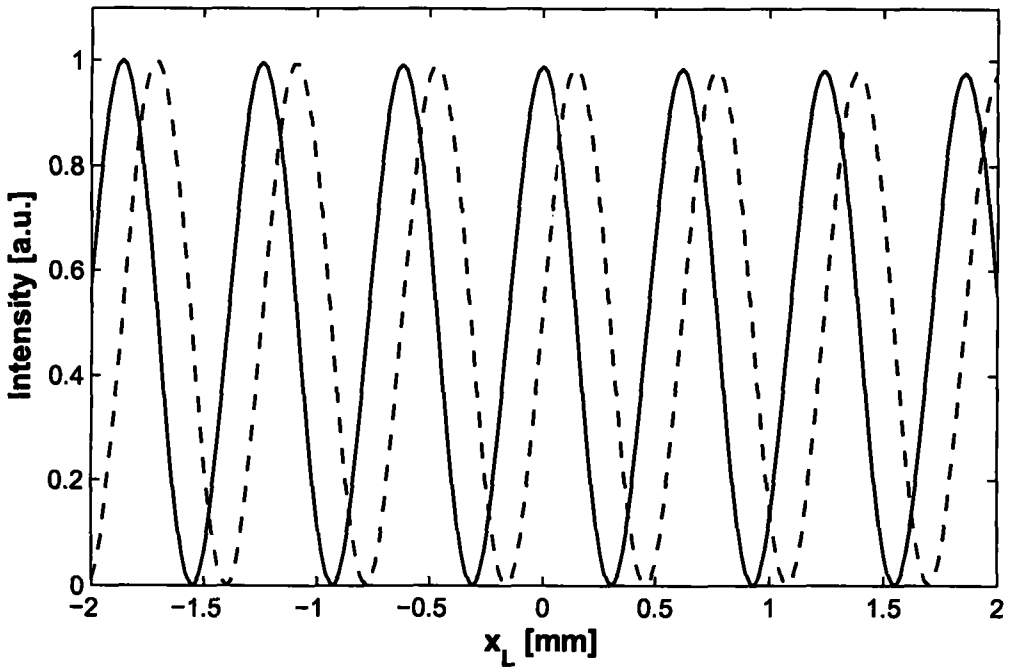

Figure 4.2: Simple ideal model: Interference pattern behind the lens for different positions of D_S. Solid and dashed line correspond to the position of detector D_S behind the double slit $x_S = 0$ and 0.15 mm.

orthogonal incident wave vector, creates the interference pattern behind the double slit represented by the solid line in *Figure 4.1*. It is obvious, that by fixing D_S in the position $x_S = 0$ mm, the weight of wave vector orthogonally incident to the lens is maximal. Then we slightly change the position of D_L. This new position corresponds to another wave vector impacting the lens, whose conjugated mode creates another interference pattern behind the double slit (lets say the dashed line in *Figure 4.1*). The contribution of this wave vector in the point x_L is again given by the detector D_S. As it can be seen from *Figure 4.1*, this contribution is however weaker then the contribution of wave vector at $x_L = 0$ mm (dashed line reaches smaller value in $x_S = 0$ mm than the solid line), and so on. We, in fact, create the image of interference pattern behind the double slit.

Finally, we should remark, that the visibility in both discussed cases, either fixed D_L or fixed D_S, reaches its maximal value. This is what one could expect, considering all used idealizations.

wave length of the pump beam in the air	λ_0	=	351.1 nm
radius of the lens	R	=	3.83 cm
focal length	f	=	86 cm
width of the slits	l_x	=	75 μ m
distance between the slits	a	=	0.255 mm

Table 4.2: Numerical values of parameters used in the experiment

4.2 Realistic approximation

The simple ideal model predicts an ideal visibility of interference patterns, which is not accomplished in reality. Unlike the ideal model, our realistic approximation involves more realistic assumptions, such as finite extent of used elements (pump laser beam, crystal, lens, double slit). We still consider the use of ideal point detectors.

Experiment we discuss has been already carried out [13]. Our study is aimed at an experimental setup and device parameters suited for a intended experiment by the Laboratory of optics in Olomouc. Naturally, the setup used in Vienna is slightly different, so that we can compare our predictions with their data only qualitatively. The differences are the use of different parameters, see *Table 4.2*, and namely another orientation of the double slit. In the experiment described in [13], the double slit is rotated by $\pi/2$. This should not, however, cause the principle changes in observed interference, compared to our orientation of the double slit.

We find it convenient to directly compare our predictions with experimentally obtained results [1]. Some of our predictions are not compared with experimental results. In such a case, we did not dispose of the particular experimental data. Our aim is to show the principle agreement with experiment, not to compare the specific quantities.

4.2.1 Double point correlator

Similarly to the ideal model, we start with a simple example, in which we fix the detector behind the lens in its focal plane and we detect the signal behind the double slit. Here we choose one curve as the reference. All curves are then normalized

[1] Unfortunately, we dealed with the experimental data a short time before finishing the thesis. Hence it was not in our capacities to do more complex comparison with experiment

to the area of reference curve. The area is calculated as integral from the curve in the interval $(-\infty, \infty)$. In other words, the curves are normalized to the probability of detection. The result is presented in *Figure 4.3*.

Lets discuss the main features of our results. First, the interference patterns agree with our expectations. Adjacent maxima of each curve show out the fall in the direction from the main maximum (see section 2.5.3). Next, the shift of fringes in dependence on the position of D_L is also obvious. The direction of this shift is again in agreement with the momentum conservation law as described in previous section. The principle agreement with experimental data is evident.

Other feature, which is worth notice, is the decrease of intensity with increasing position of D_L. Our imaging elements (the double slit and the lens) are adjusted in such a way, that the two wave vectors, which are orthogonally incident on the lens and on the double slit, satisfy the momentum conservation law. Our model thus predicts, that the farther our detector D_L from the lens axis is, the weaker is the contribution of the mode impacting the double slit. Practically it means, that we would have to measure longer time to receive an interference pattern with comparable counts of events.

We now repeat the same experimental setup, but we fix the detector D_L in the distance $z_L = 2$ m, i.e. in $2f$ behind the lens. The results are shown in *Figure 4.4*. The most interesting feature of the result is undoubtedly the disappearance of interference. This surprising result could be better understandable after reading the section 4.2.2.

Next we investigate the setup with fixed D_S. The detector D_L is placed in the focal plane of the lens. The result is shown in *Figure 4.5*.

Here again, the explanation of what we observe is quite analogous to the explanation for the simple ideal model. The major features are the shift of fringes in dependence on the position of D_S and the decrease of intensity. The principle agreement with experimental data is also evident.

The dependencies plotted in *Figure 4.3* and *Figure 4.5* are just the special cases of our correlator, which is the function of two variables x_L and x_S. The overall situation is shown in *Figure 4.6*. The continuous shift of interference fringes is obvious in both cases. Either we continuously change the position of D_L and detect the signal behind the double slit or vice-versa. Corresponding interference pattern for particular position of D_L is then the cross section in the $x_S - Intensity$ plane. Similarly, we can continuously change the position of D_S and detect the signal behind the lens. The particular field distribution is then given by the cross section in $x_L - Intensity$ plane. Specifically, the cross sections marked by solid lines correspond to the interference patterns shown in *Figure 4.3*, those marked by dashed lines correspond to the field distributions plotted in *Figure 4.5*.

Finally, we should say, that our realistic approximation gives in a particular limit the same results as the ideal model. By increasing sufficiently the width of

crystal, the width of the pump beam and decreasing sufficiently the width of slits, we receive the interference patterns with perfect visibility and no intensity fall. One can also see, that the simple ideal model gives some basic predictions (period of interference fringes), but is not suitable for a more accurate description of a realistic experiment.

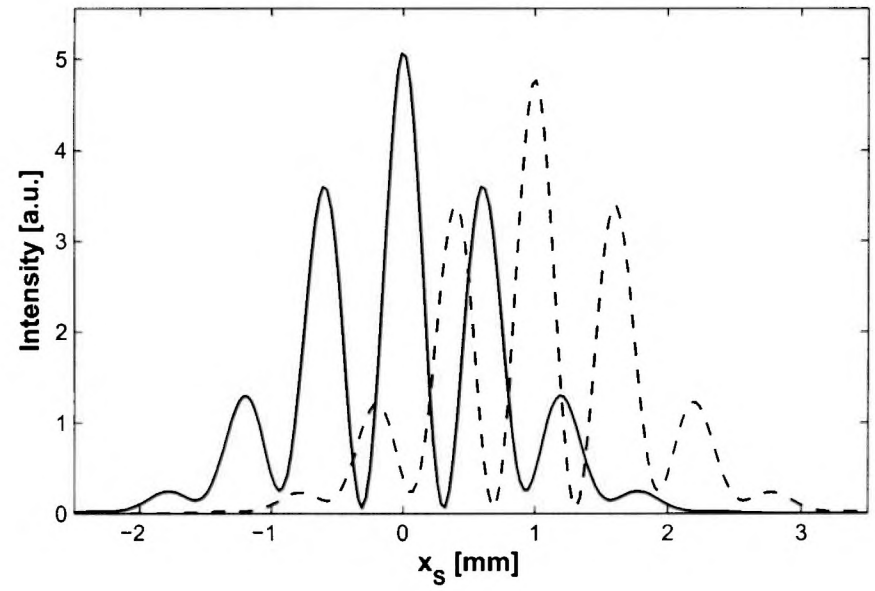

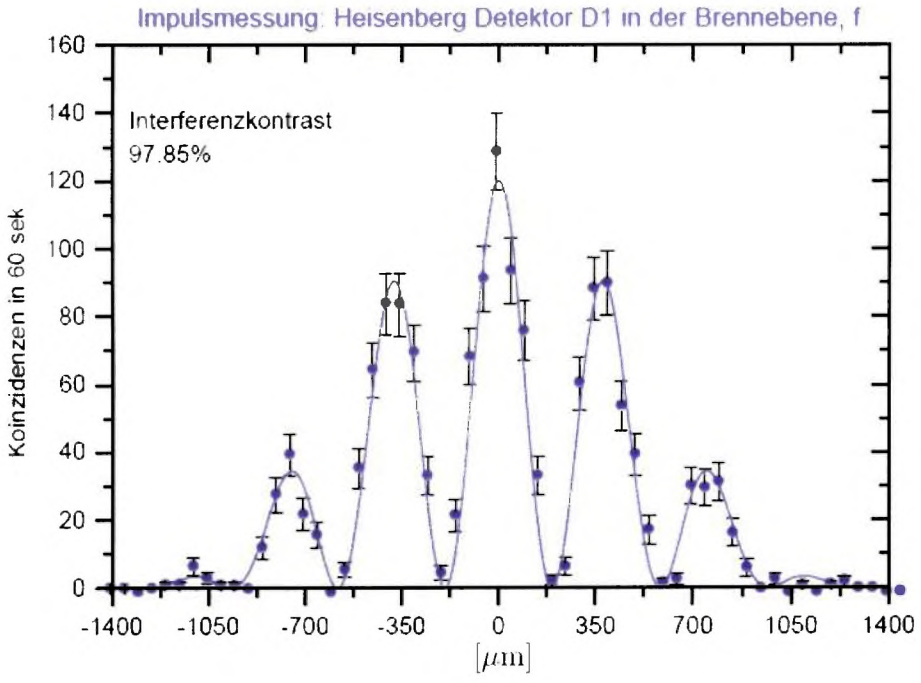

Figure 4.3: Interference pattern behind the double slit. D_L is fixed in the position x_L.
Upper image: Realistic approximation. The solid line corresponds to $x_L = 0$ mm and the dashed line to $x_L = 1$ mm.
Lower image: Experimental results for $x_L = 0$ mm.

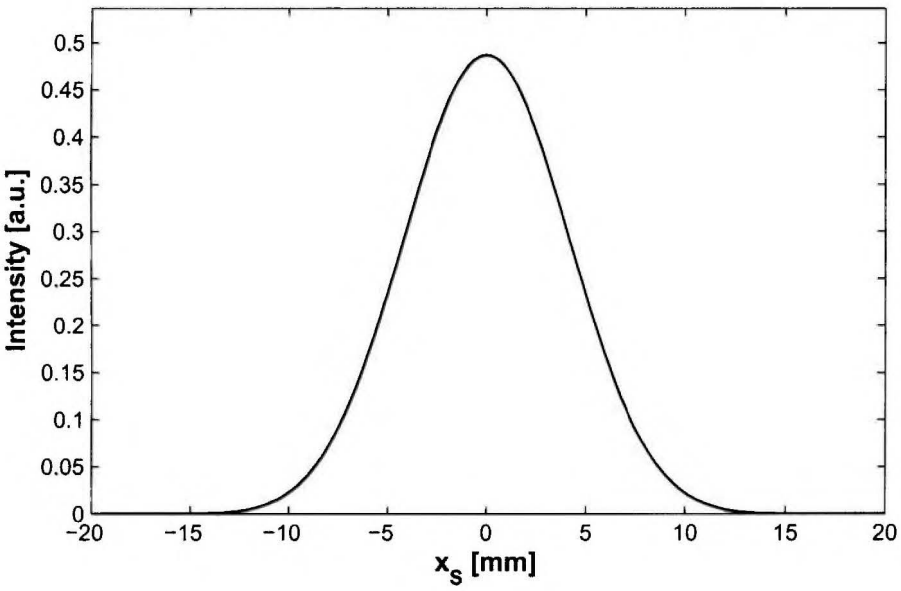

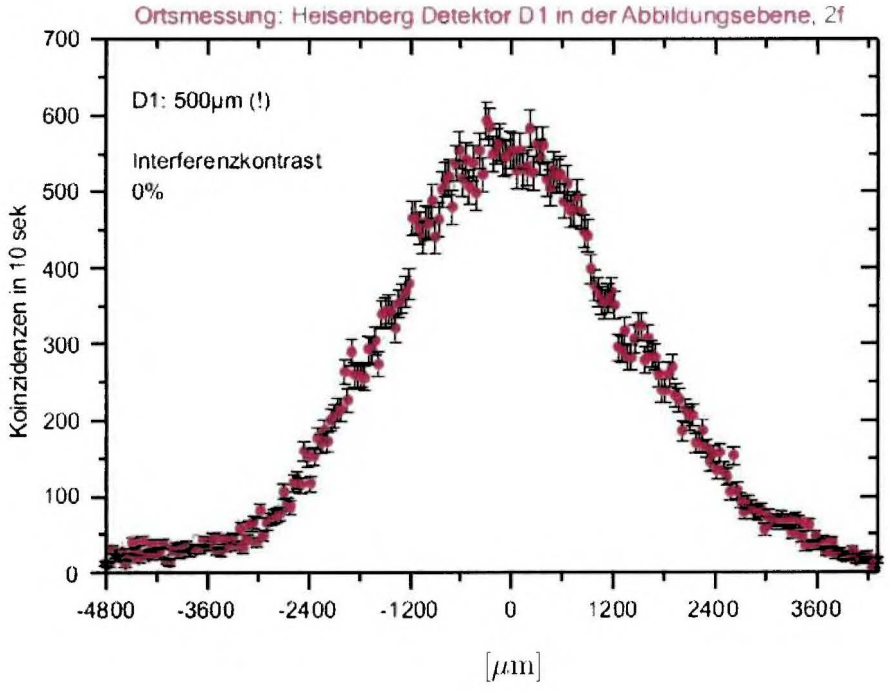

Figure 4.4: Interference pattern behind the double slit. D_L is fixed in the position $x_L = 0$ mm at distance $z_L = 2f$.
Upper image: Realistic approximation.
Lower image: Experimental results.

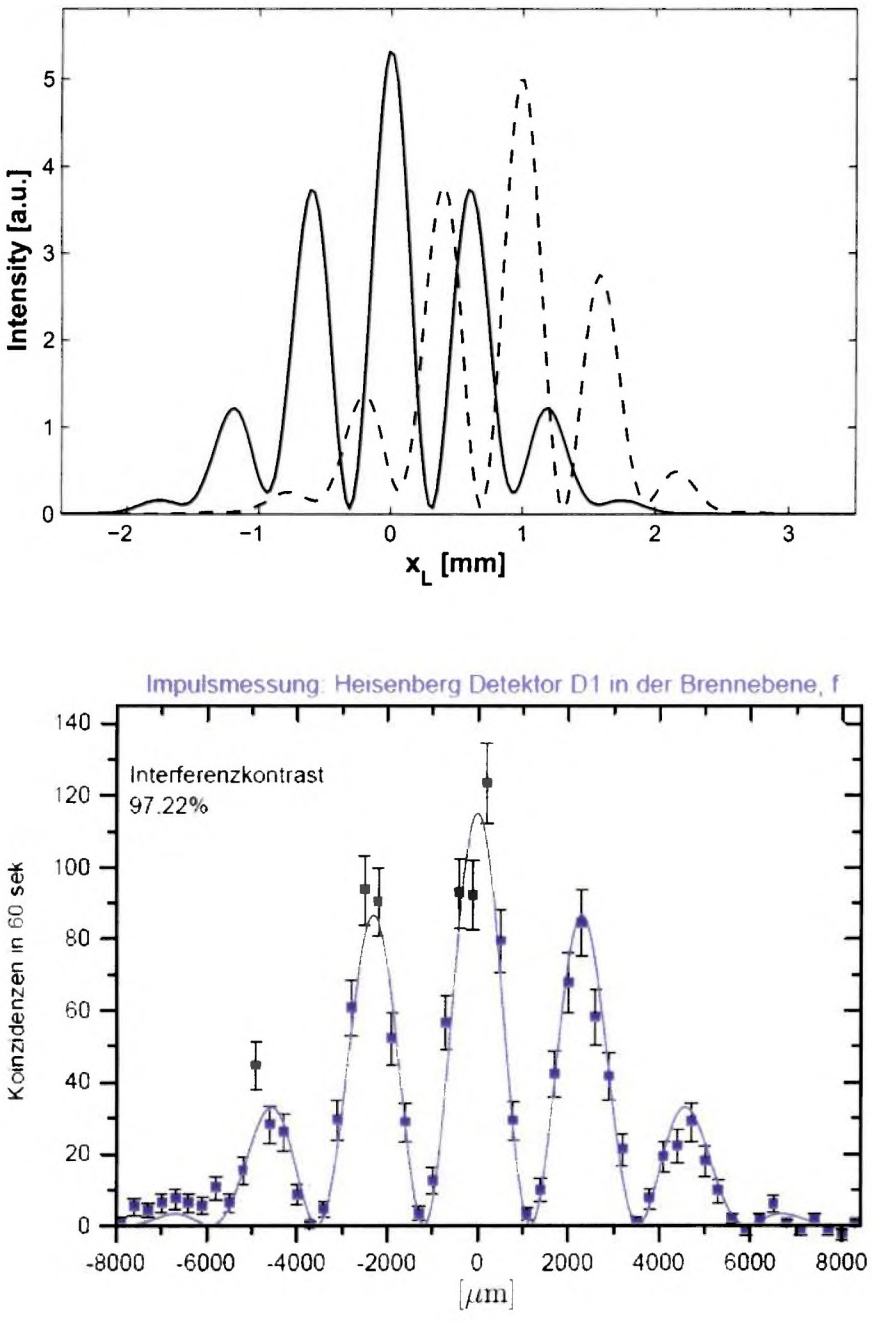

Figure 4.5: Field distribution in the focal plane of the lens. D_S is fixed in the position x_S.
Upper image: Realistic approximation. The solid line corresponds to $x_S = 0$ mm and the dashed line to $x_S = 1$ mm.
Lower image: Experimental results for $x_S = 0$ mm.

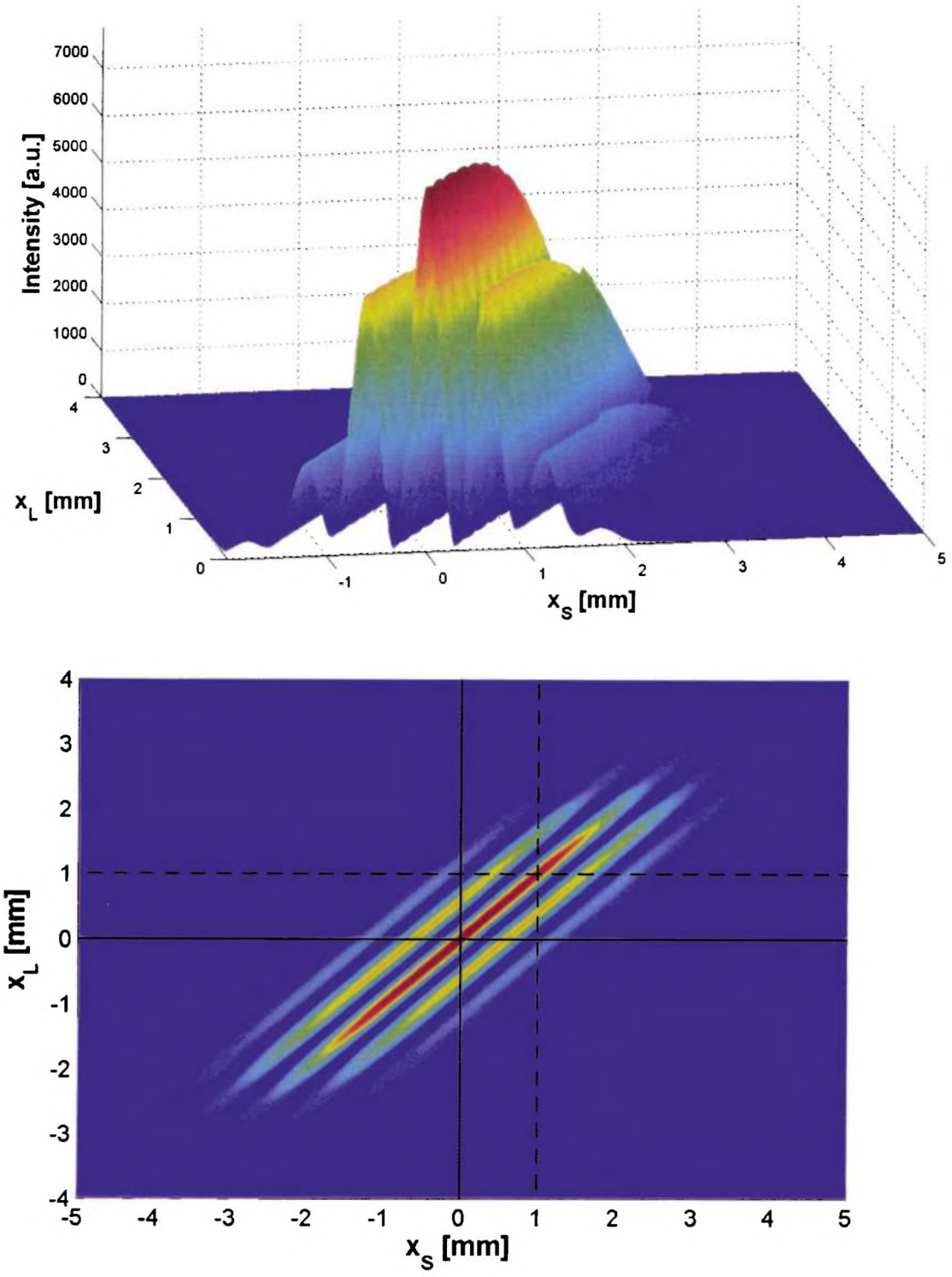

Figure 4.6: Dependence of the correlator on the position of both detectors.
Upper image: Detailed view of the correlator structure.
Lower image: Floor projection of the correlator. Horizontal cross sections are plotted in *Figure 4.3*, vertical cross sections are plotted in *Figure 4.5*.

4.2.2 Out of the focal plane

As we have seen above, there is a principle difference between patterns observed in the focal plane and out of the focal plane. A very interesting question is, how looks the field distribution in a general distance z_L behind the lens and how it is connected with the other optical element, in our case with the double slit. Lets start directly with a general situation presented in *Figure 4.7*.

We can obtain the particular field distribution behind the lens as the cross section in the $x_L - Intensity$ plane. As we can see, besides the interference patterns, whose shapes are similar to those shown in *Figure 4.5*, at a particular distance, we get the image of the double slit. For the present setup, this distance is $2f$. If we accept that the non-linear crystal acts as a "mirror", the double slit is in an effective distance $d_L + d_S$ from the lens. We then see that the image is created exactly in the image plane. This is a surprising result arising from the quantum entanglement - we are able to visualize the object with photons, which never passed through this object. The chosen cross sections, marked by solid and dashed line, are plotted in *Figure 4.8*. The experimental result confirms, that the image of the double slit is really created in the image plane of the lens.

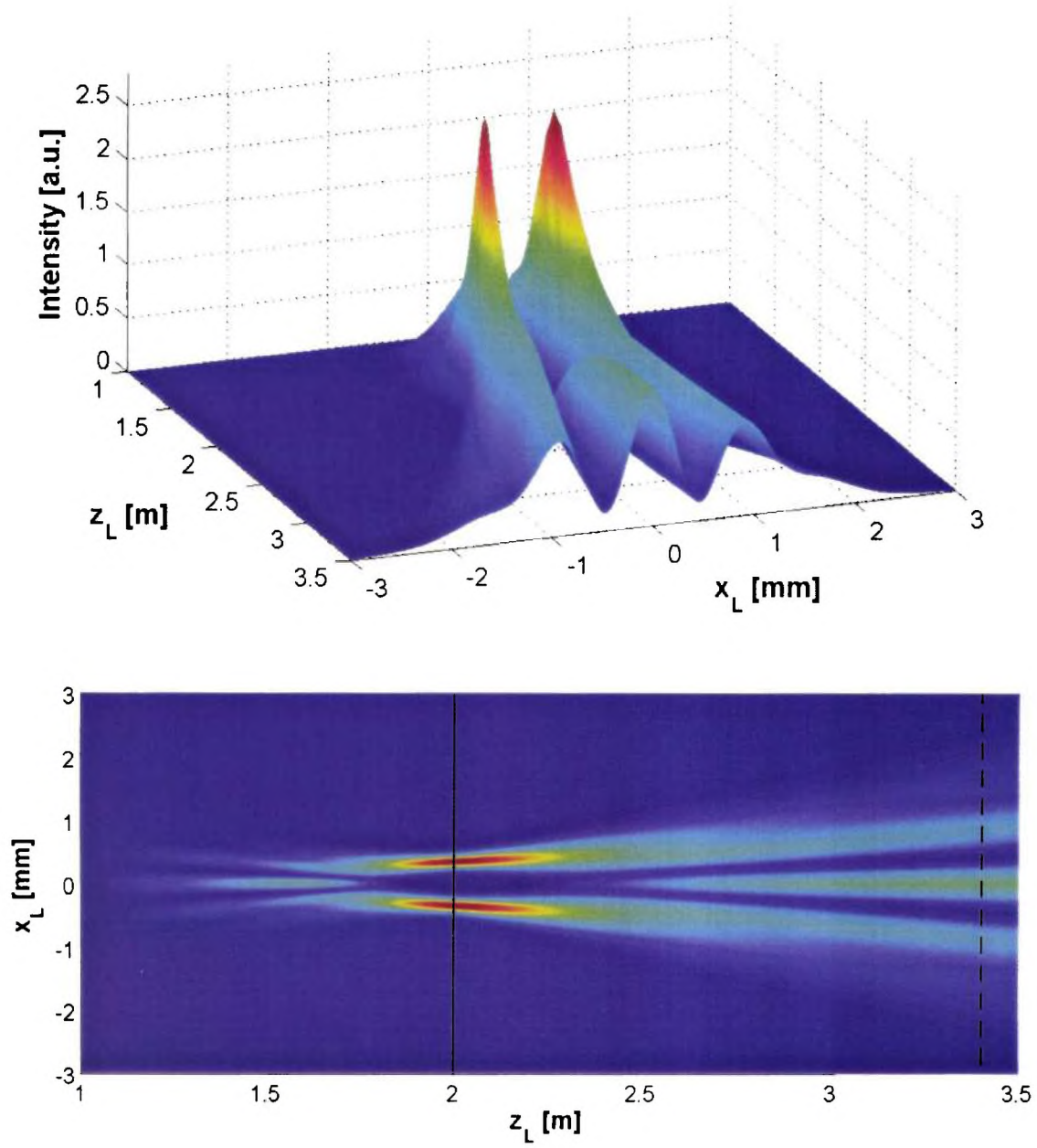

Figure 4.7: The field distribution behind the lens. The detector D_S behind the double slit is fixed in the position $x_S = 0$ mm.
Upper image: 3D view of the field distribution.
Lower image: Floor projection of the field distribution. Solid and dashed line cross sections are plotted in *Figure 4.8*.

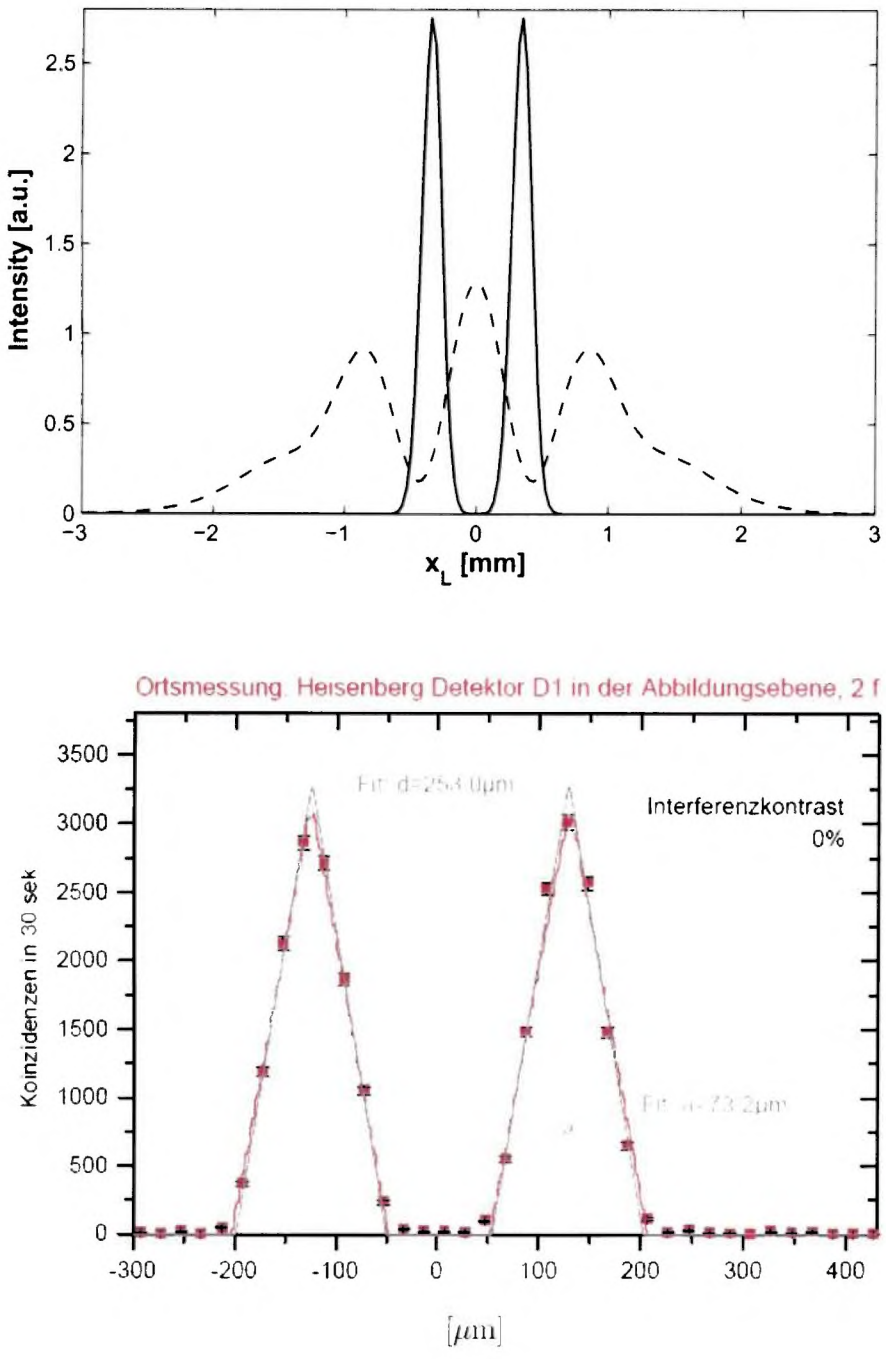

Figure 4.8: Field distribution behind the lens. D_S is fixed in the position $x_S = 0$ mm. *Upper image:* Realistic approximation. Solid line corresponds to the position of the detector behind the lens $z_L = 2f = 2$ m and the dashed line to $z_L = 3.4$ m. *Lower image:* Experimental results for $z_L = 2f$.

Chapter 5

Summary

The phenomenon of quantum entanglement has been already known for several decades. More complex forms of the entanglement, like those which can appear at multi-photon states, were not observed until recent past, when the progress in experimental techniques made it possible to investigate this feature of quantum mechanics in laboratory conditions. One of these new methods uses two-photon states to measure the relationship between the wave vector domain and the space domain, i.e., quantities related by the traditional Heisenberg relation of uncertainty. These setups are briefly called Heisenberg microscope.

So far, there are not many optical experiments of this kind. In the same time, there is a lack of theories exploring this problem. The presented diploma work is aimed to fill this gap in theory offering a convenient description with the basic realistic features included.

We considered an experiment with one entangled photon pair, where each photon propagates in a separate imaging system. The first system contains the lens, the other the double slit. The natural theoretical tool to describe the relationship between the space frequency and space domains, or the relationship between the two photons, is the two-photon correlator. Our aim was thus to evaluate the correlator of this particular experiment.

Former studies have interpreted experimental data with the help of a very simple model, which does not cover important realistic features of the experiment, such as the finite extent of the pump laser beam, of the crystal or of the slits. We have developed a description, which involves these features in an approximation leading to semi-analytical theory.

Using approximations in spirit of the stationary phase approximation, which keep the main physical characteristics and avoid the complications during the calculation of correlator, we were able to obtain the analytical result. This result is however relatively complicated as it is given by the inversion of a 6×6 matrix.

While an explicit analytical formula would be very lengthy, a numerical treatment is very easy.

As we have shown, our model provides us with predictions, which are in very good agreement with experiment. Therefore it seems, that our model is suitable to predict the realistic results of this type of experiment.

References

[1] Internet: http://en.wikipedia.org/wiki/Quantum_entanglement, Wikipedia the free encyclopedia, 2006.

[2] Dušek M.: *Koncepční otázky kvantové teorie*, Univerzita Palackého v Olomouci, Olomouc, 2002.

[3] Dusek M., Soubusta J., Perina J. Jr., Hendrych M., Haderka O., Trojek P.:*Experimental verification of energy correlations in entangled photon pairs*, Physics Letters A 319, 251 (2003).

[4] Dušek M.: Czech Journal of Physics **46**, 921 (1996).

[5] Franson J. D.: Physical Review Letters 62, 2205 (1989).

[6] Loudon R.: *The Quantum Theory of Light*, Oxford University Press, 2000.

[7] Davydov A. S.: *Kvantová mechanika*, SPN, Praha, 1978.

[8] Mandel L., Wolf E.: *Optical Coherence and Quantum Optics*, Cambridge University Press, 1995.

[9] Saleh B. E. A., Teich M. C.: *Základy fotoniky 1*, Matfyzpress, Praha, 1994.

[10] Goodman J. W.: *Introduction to Fourier optics*, McGraw-Hill, Inc., 1968.

[11] Kvasnica J.: *Teorie elektromagnetického pole*, Academia, Praha, 1985.

[12] Abramowitz M., Stegun I. A.: *Handbook of Mathematical Functions*, Dover Publications, Inc., New York, 1970.

[13] Dopfer B.: *Zwei Experimente zur Interferenz von Zwei-Photonen Zuständen Ein Heisenbergmikroskop und Pendellösung*, Doktorarbeit zur Erlangung des Grades eines Doktors an der Naturwissenschaftlichen Fakultät der Leopold-Franzens Universität Innsbruck, 1998.